PENNSTATE

Center for Advanced Materials

The Characterization of Microbiologically Influenced Corrosion (MIC) Under Cathodic Protection Conditions

Annual Technical Report
for the Period October, 1995 to October, 1996

Grant No: N00014-94-1-0027
R&T Project: cor 5251---01
S.O. Code: 331
Disbursing Code: N00179
Ago Code: N66005
Cage Code: 7A720

Principal Investigators:

Dr. Digby D. Macdonald
Dr. Richard Unz

Researchers:

Michael J. Morgan
Richard A. Royer

College of Earth and Mineral Sciences

OBJECTIVES

The goal of the present research is to investigate the effectiveness of cathodic protection in preventing, halting, or limiting the microbiologically influenced corrosion (MIC) of carbon steel substrates in seawater. MIC is defined as the corrosion resulting from the interaction of bacteria, especially Sulfate Reducing Bacteria (SRB), and their biological end products with metal surfaces. In order to address this problem, four key issues are being investigated. Firstly, the chemical and electrochemical conditions beneath biofilms must be determined. Secondly, the thermodynamic conditions necessary at the surface of the substrate for cathodic protection to be effective must be known. Thirdly, the process by which SRB colonize and adhere to steel surfaces needs to be examined. Finally, the effectiveness of impressed current cathodic protection techniques on inhibiting corrosion due to the presence of biofilms and tubercles on the carbon steel surface must be investigated.

INTRODUCTION

MIC is a common occurrence on metal substrates exposed to marine environments. Biofilms formed on metal surfaces frequently contain microorganisms whose metabolic end-products react with the metal substrate to increase corrosion rates. SRB are anaerobic bacteria, meaning they utilize reduced inorganic forms of sulfur as electron acceptors at low (negative) oxidation reduction potentials but may persist in

intramolecular oxidation of organic substrates, e.g., lactate and pyruvate. They can survive in environments containing oxygen, but truly thrive in an oxygen-free atmosphere. Thus, a biofilm that contains SRB must produce an oxygen gradient within the film to allow the SRB to live and be active. As a result, SRB are typically found in the lower regions of the biofilm, closest to the metal substrate, where the concentration of oxygen is very low. Since SRB are not found alone in nature, a mixed consortia of bacteria with various metabolic compositions are found within biofilms. The metabolic activities of these different bacteria create microenvironments within the biofilm which permit optimum activity among the different bacteria.

Bacteria typically have dimensions of less than 0.2 to several hundred μm in length by up to 2 to 3 μm in width.[1] Their small size allows them to enter crevices or pits with a great amount of ease. As bacteria colonize a steel surface, an oxygen concentration cell develops, where the area underneath the bacterial colony is deprived of oxygen relative to the outer surface, which is exposed to an oxygenated environment. Thus, the area under the bacterial deposit becomes anodic and the outer surface becomes cathodic, leading to localized corrosion of the area under the bacterial colony. This form of corrosion is known as differential aeration cell corrosion, concentration cell corrosion, or crevice corrosion.

Under anaerobic conditions, SRB such as *Desulfovibrio desulfuricans* utilize the sulfate ion (SO_4^{2-}) as the terminal electron acceptor in the metabolism of nutrients. This leads to the production of hydrogen sulfide, H_2S. The following reactions were proposed for the MIC of iron by Von Wolzogen Kuhr and Van der Vlugt[2] in 1934:

$$4Fe \rightarrow 4Fe^{2+} + 8e^{-} \qquad (1)$$

$$8H_2O \rightarrow 8H^+ + 8OH^- \quad (2)$$
$$8H^+ + 8e^- \rightarrow 8H_{ads} \quad (3)$$
$$SO_4^{2-} + 8H \rightarrow S^{2-} + 4H_2O \quad (4)$$
$$Fe^{2+} + S^{2-} \rightarrow FeS \quad (5)$$
$$4Fe + SO_4^{2-} + 4H_2O \rightarrow 3Fe(OH)_2 + FeS + 2OH^-. \quad (6)$$

The critical reaction is reaction (4) where SO_4^{2-} is utilized by SRB to produce S^{2-}. However, under anaerobic conditions, it is likely that the cathodic reduction of H_2S,

$$H_2S + 2e^- \rightarrow H_2 + S^{2-} \quad (7)$$

and the formation of iron sulfide from iron metal,

$$Fe + S^{2-} \rightarrow FeS + 2e^- \quad (8)$$

lead to the increased corrosion rates. The iron sulfide layer is considered to be an ideal cathodic site for the reduction of oxygen and thus leads to the acceleration of the anodic reaction on the steel surface under the biofilm or deposit.[3] The primary film formed during biogenic corrosion is mackinawite, $Fe_{1+x}S$.

Other bacteria may also contribute to the corrosion of the underlying steel substrate. Many strains of bacteria, such as *Thiobacillus thioxidans* and *Clostridium aceticum* produce sulfuric acid and acetic acid, respectively. The production of acid near the metal surface can and does lead to increased corrosion rates. Iron oxidizing bacteria such as *Gallionella sp.* oxidize ferrous ions to ferric ions to obtain energy.[3] These bacteria are also often found in consortia with SRB. The possibility of hydrogen embrittlement by the increased absorption of atomic hydrogen into the steel due to the production of hydrogen sulfide is another deleterious effect caused by MIC. H_2S produced by SRB may be oxidized to elemental sulfur, which is also corrosive to carbon steel, particularly under anaerobic conditions.

Biofilm Development

The development of a biofilm on a steel surface is the first step in the development of microbiologically influenced corrosion. It is therefore logical that an investigation of MIC should begin with an investigation of biofilm formation and characteristics. It has been estimated that the vast majority of bacteria in nature are found within biofilms rather than in a planktonic state[4]. Growth within a biofilm is advantageous relative to planktonic growth because it confers a number of ecological advantages such as enhanced nutrient scavenging ability, protection from environmental changes, provision of a genetic pool and genetic exchange, an extended residence time for the metabolism of difficultly degradable substances, as well as an allowance for the development of microconsortia[5].

The formation of a biofilm begins with the adhesion of cells to the substratum. The nature of the substratum affects the mechanism of bacterial attachment. Surface properties, which can also affect adhesion, include surface charge, surface free energy, and surface roughness[6,7]. These factors encompass the effects of hydrophobicity and protection from turbulent flow. The surface characteristics of a material are subject to change by their environment. Therefore, when a material is immersed in a solution, the surface charge and surface free energy are subject to change[6]. An example of the alteration of surface charge is the change due to the adsorption of organic molecules to surfaces immersed in seawater. These organic molecules may also serve as nutrients for bacteria initially colonizing a surface and the organic layer will change from a hydrophobic to a hydrophilic character.

Adhesion in relatively unpolluted waters is typically divided into reversible and irreversible stages with the former generally thought to be a preliminary form of adhesion[6]. The difference is largely the shift from the weaker van der Waal attractive forces of reversible adhesion to the more strongly oriented bridging polymers promoted by adjacent metal ions and covalent bonding in what is termed irreversible adhesion. Polymer bridging is considered one of the principle mechanisms of adhesion in biofilm formation. Bridging polymers are proteins and polysaccharides, but distinct cell appendages, e.g., fimbriae, are thought to have a role in anchoring cells to the substrate[6]. As these bridging polymers differ from cell to cell, it is reasonable that adhesion is cell-dependent and thus, dependent on the physiological state of the cell. These extracellular polymers are basically acidic polysaccharides containing functional groups that bind metals.[3] These substances serve to hold the biofilm onto the metal surface, trap corrosion products at the metal/biofilm interface, and decrease diffusion to the metal surface.

The initial colonization stage of biofilm formation is characterized by a low bacterial density and a minimal competition between organisms. This low competition favors R-strategists, or organisms with high growth rates. The transition stage occurs next, where the cells produce exopolymeric material in which they become enmeshed. Competition within the film increases with population density and organisms with higher competitive abilities, K-strategists, increase in importance. Finally, in the mature biofilm, the population density and competition are both high, and the K-strategists predominate.

Complex interactions occur within a mature biofilm, and the exact mechanism of MIC is difficult to obtain, as more than one mechanism is likely at work. Thus, a

simplification of such a system should serve as the starting point for the investigation of the corrosion of carbon steel in marine environments.

EXPERIMENTAL

Cell

The experimental cell consists of the three electrodes common in electrochemical studies, namely, the working, reference, and counter electrodes, as seen in Figure 1. The working electrode, WE, is a 5.08 cm diameter 1018 carbon steel disk polished to a 600 grit finish with silicon carbide polishing paper, surrounded by a 10.16 cm outer diameter 1018 carbon steel ring, polished in the same manner. The two are separated by a thin strip of polyester epoxied to the inner circumference of the ring. The two steel samples are mounted with epoxy onto a Plexiglas base and rest in a 190 mm by 100 mm petri dish. Electrical leads are connected via silver epoxy onto the carbon steel disk and ring for current and potential measurements. The reference electrode, RE, is a Fisher™ Saturated Calomel Electrode (SCE). The counter electrode, CE, is a 0.51 mm diameter platinum wire around the periphery of the cell.

Atop the inner carbon steel disk is placed a 1.905 cm thick disk of transparent Plexiglas of identical diameter as the disk. This is the crevice "former". The former is supplied with screws in order to adjust the crevice width, as can be seen in Figure 2. Additional screws are epoxied onto the ring for additional support and to prevent the former from moving radially, laterally, and/or normally, which would disrupt the crevice

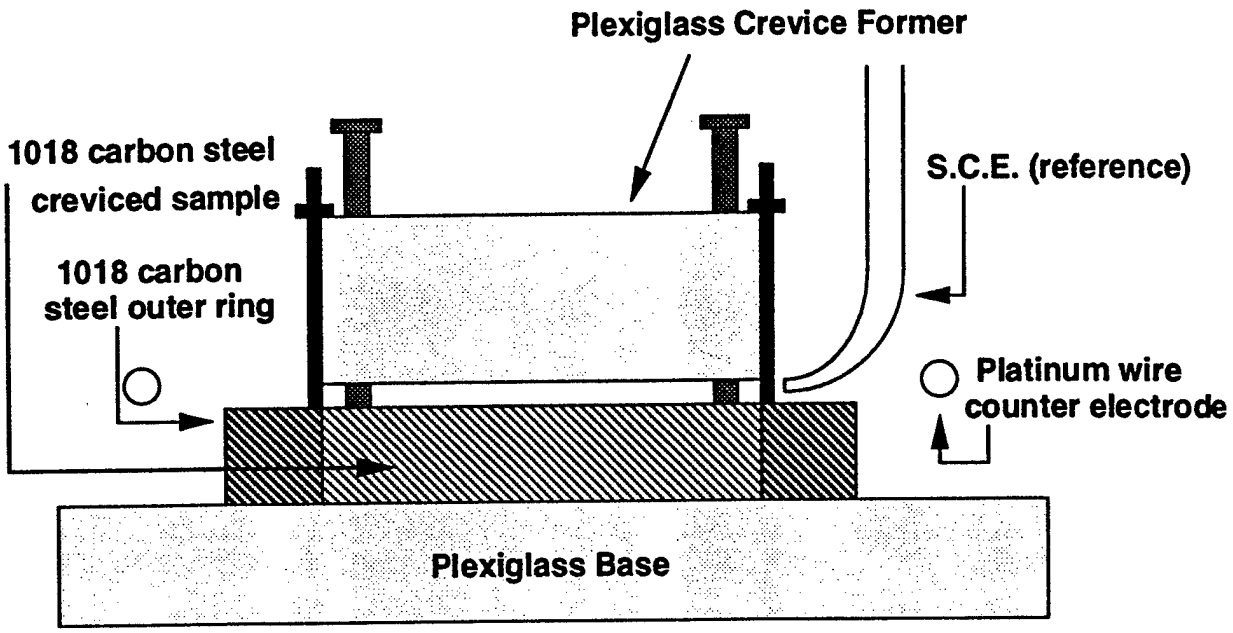

Figure 1: Crevice corrosion cell simulating a tubercle adhering to a steel surface.

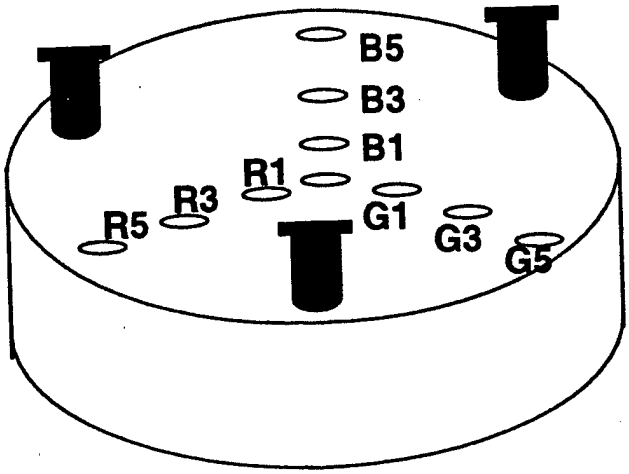

Figure 2: Diagram of Crevice Former arrayed with holes at various distances from the crevice center.

environment. The transparent nature of the former allows for direct viewing of the crevice environment.

The crevice former is arrayed with holes so as to allow measurements of pH and potential at different sites within the crevice. pH is measured with Ag/AgCl combination pH/reference microelectrode probes and potential is measured with separate Fisher™ Saturated Calomel Reference Electrodes in Luggin capillaries containing agarose salt bridges. Rubber plugs are used to prevent oxygen from entering the crevice through holes not being used for measurements. There is also a central hole in the former to allow flow of corrosive solutions such as sodium sulfide or SRB inoculated solution.

A Gamry™ potentiostat is used to polarize the WE to a specified potential, simulating cathodic protection, and hence rendering the working electrode immune to corrosion (or at least limiting the rate of attack). A Keithley™ picoammeter is used to measure the current flowing from the crevice to the outer ring during open circuit and a Keithley™ multimeter is used to measure potentials within the crevice. This cell is designed to produce an oxygen concentration cell similar to those produced by tubercles in MIC. The Plexiglas crevice former simulates the bacterial colony or biofilm and the flowing solution simulates the production of metabolic end-products by the SRB. The steel disk represents the area under the bacterial colony and the steel ring serves as the surface outside the deposit. A 3.5 weight percent sodium chloride (NaCl) solution is used as the bulk solution to simulate seawater.

Electrophoresis

The computer-controlled electrophoresis system that was purchased is being used to analyze the protein composition of the bacteria to be used in upcoming experiments. The system allows both one-dimensional and two-dimensional separations to be carried out. The one-dimensional technique currently being used is sodium dodecylsulfate poly acrylamide gel electrophoresis (SDS-PAGE). This technique separates proteins based only on molecular weight, rather than on both molecular weight and charge. When the presence or absence of a known protein is to be evaluated, this technique may be used to search for a protein of the correct molecular weight. Evaluating the presence or absence of specific hydrogenases of known molecular weight is an example the usefullness of this technique.

Two-dimensional gels allow for the separation of a greater number of proteins. The current two-dimensional method being evaluated employs isoelectric focusing (IEF) in one dimension and SDS-PAGE separation in the other. The use of IEF coupled with SDS-PAGE allows separation, first, by isoelectric point, and then by apparent size. Employing two separation parameters allows for greater discrimination between similarly sized proteins than the one-dimensional SDS-PAGE affords.

Analysis of Electrophoresis Data

Analysis of one-dimensional gels involves comparison of samples with known molecular weight protein standards, and subsequent calculation of the molecular weights

of the component proteins of the standard. The primary use of this method in the present study will be for detection of known proteins that may be critical in determining the validity of various proposed biocorrosion mechanisms. The usefullness of this technique will be in detecting proteins that have been considered important in biocorrosion and have been characterized in terms of molecular weight. As the study progresses, unknown proteins found to appear significant from two-dimensional gel analysis may be tested by one-dimensional analysis as well.

The analysis of two-dimensional gels will yield isoelectric point and molecular weight estimations for proteins detected by comparison with standards. In a two-dimensional system, these two characteristics can be given a set of Cartesian coordinates. Any protein may therefore be identified by a unique set of coordinates. The resulting data for a given gel with then be in the form of proteins present, as identified by the coordinates, and, therefore, provide values for the isoelectric point and molecular weight. The profile of proteins present under a given set of growth conditions for a particular species can then be compared to profiles recorded for other growth conditions and for other species. A scanner and image analysis software may be used to aid in evaluating the gels. Digitized or digital photographs of gels may be employed as an alternative for conversion of gels into digital images. If neither of these techniques is practical, manual analysis of the gel photographs will be necessary. An advantage of image analysis software is the ability to quantify protein based on color intensity. Currently, software and hardware availability is being investigated.

Comparison of the proteins present under different growth conditions is to be conducted. In addition, the effect of cells possessing those proteins on the severity of

corrosion in the crevice is to be investigated. The protein composition of cells is strongly affected by growth conditions such as medium components and growth rates. By studying the relationship between growth rate, protein composition and corrosion rate, a better understanding of the mechanisms of MIC may be gained. The use of the chemostat allows manipulation of growth rate and medium composition, permitting cells to be repeatedly produced with a given suite of proteins.

Cultures

Cultures of three marine sulfate reducing bacteria have been obtained from the American Type Culture Collection (ATCC). All three are members of the genus *Desulfovibrio*. *Desulfovibrio desulfuricans aestuarii* (ATCC #29578) has been cultured successfully in batch culture in two different media. Medium C from Postgate[8] has been selected for batch and continuous culture. The medium has been modified by the addition of 0.6 g/l of cysteine hydrochloride as a redox poising agent.

Experiments with batch cultures established that after several weeks in medium C, *Desulfovibrio desulfuricans aestuarii* (ATCC #29578) produced exopolymeric material such that the culture contained a large floc of cells embedded in this material and the material required very vigorous shaking to disperse the floc. It appears that the conditions in the batch cultures after several weeks favored exopolymer production. The experiments clearly demonstrated the ability of this strain to produce copious quantities of exopolymeric material under appropriate conditions.

Experiments are being conducted which will determine under what conditions exopolymer production is favored. These experiments will involve the chemostat to control the growth rate of the cells and the chemical composition of the medium. These studies may be supplemented by batch culture experiments. The other strains will be tested for polymer production under the same conditions as *Desulfovibrio desulfuricans aestuarii* (ATCC #29578.

Culture Conditions

The goal of manipulating culture conditions is to observe the effect of changes induced in the bacteria by their environment on MIC. One means by which bacteria can adapt to a different environment is via inducible enzymes. The production an inducible enzyme does not occur under all growth conditions but, instead, is triggered by some environmental variable. The net result of many inducible enzyme systems being changed from "on" or "off" is a significant shift in the capabilities of the same cell under different conditions of growth. The manipulation of culture conditions such as growth rate and medium constituents allows one to reproducibly induce these changes in the metabolic capabilities of the bacteria. The means for detecting these changes in enzyme composition is through protein analysis by electrophoresis as described in the previous section. Growth rate manipulation in a chemostat is a reproducible means of inducing cellular compositional changes and is the method of choice where practicable.

Growth Rate

The use of a chemostat allows precise growth rate control by manipulation of flow rate. At steady state, the flow rate of the chemostat and the growth rate of the organism are identical. Cultures grown in a chemostat are going to be used whenever possible to allow for good reproducibility. The most environmentally relevant growth rates may, in some cases, be fairly low. The response of some cultures may be exopolymer production, which has been observed consistently in old batch cultures of *Desulfovibrio desulfuricans aestuarii* (ATCC #29578).

Chemostat kinetics do not allow for the growth of material on the vessel wall or in aggregate form. The production of polymers and low growth rate behavior are, however, both potentially very important in understanding how MIC is occurring under natural conditions. Several smaller reactors are going to be used to culture flocculating or adhering cultures. Although these reactors will not be behaving as true chemostats, they will allow control of the nutrient input into the system, by controlling flow rate and monitoring the nutrient level in the waste from the reactor. Existing biofilm kinetic models will be employed to calculate a growth rate for cells grown under such conditions.

Strain Selection

Comparisons of different strains of bacteria allow for comparisons of potentially different mechanism of MIC. Selection of highly similar strains of the same subspecies of bacteria allows for comparisons of bacteria that differ only slightly in capabilities.

Comparison of strains may indicate the relative importance of certain metabolic capabilities in MIC. Analysis of the relationship between metabolic capability or enzymology could answer mechanistic questions about exactly how bacteria cause or influence MIC. One example of this type of experiment is the evaluation of the impact of various types of hydrogenase present in closely related sulfate-reducing bacteria on MIC.

Open Circuit Crevice Experiments

In order to determine the chemical and electrochemical conditions that exist inside the crevice, a series of measurements of pH, potential, and current flow within the crevice were taken under a number of various conditions. Experiments involving crevice corrosion in simulated seawater, in simulated seawater containing sulfides, and in simulated seawater containing an agarose film were conducted following similar procedures. The goal of these experiments is to determine whether the designed cell is capable of producing a crevice environment, and if so, what are the chemical and electrochemical characteristics of that environment under the specified conditions? Once these characteristics are determined, it would be possible to determine the conditions necessary to cathodically protect against crevice corrosion, for each case, in a marine environment. A 3.5 weight percent solution of NaCl in water was used as the stagnant bulk solution and the crevice width was set at 200 μm. The experiments with sulfides involved a slow flow (2 ml/hr) of 0.05 weight percent sodium sulfide solution to simulate

the metabolic end-products of SRB, and agarose was allowed to cool within the crevice to simulate the physical presence of a biofilm.

Cathodic Protection Experiments

Once a crevice was developed, a series of cathodic protection experiments were run on the same cell orientation to determine its effectiveness in halting or slowing the progression of corrosion. These experiments were performed using potentiostatic methods, in which the potential of the working electrode is held constant by adjusting the amount of current supplied to the working electrode. The reference electrode in this setup is placed at the mouth of the crevice. The equilibrium potential of the working electrode is taken to be -0.682 V vs. SCE. A constant potential of -0.7755 V vs. SCE was applied to both the sample in the crevice and the outer surface, and pH, potential, and current were monitored. This value for the protection potential corresponds to that which has been accepted for the cathodic protection of carbon steel in marine environments, without consideration of the effects of SRB[10]. When sulfides were introduced into the system, a constant potential of -0.8755 V vs. SCE was applied to the WE, as per that which has been accepted in the literature for cathodic protection of carbon steel in the presence of SRB[10].

Following the cathodic protection experiments, electrochemical impedance experiments were run to characterize the steel/electrolyte interface within the crevice. The alternating voltage perturbation amplitude was 5 mV peak to peak in addition to the direct

protection potential within a frequency range of 5000 Hz to 100 μHz. Impedance runs were made on the cells with injected sulfides and with the agarose film.

Data Acquisition

Collection of current, pH, and potential data is performed by an IBM compatible personal computer. The bulk of the data is collected by a Cyrel 08, eight channel, twelve bit analog to digital conversion board (ADCB). Most signals are routed through a Cyrel 16, sixteen channel relay board containing sixteen form-c opto-mechanical relays. The ADCB reads potential relative to three reference electrodes that are in close proximity to the disk inside the crevice, with one reference electrode external to the crevice monitoring the potential of the outer ring. The ADCB also records voltages generated by four pH microelectrodes arranged in a similar manner. The ADCB also reads current output from a Keithley model 480 picoammeter. Data acquisition is coordinated by two computer programs, one for the potentiostat, and a custom program which controls the relay board and ADCB.

The suite of four reference electrodes that are connected to the ADCB are selected to be read individually and are used to determine the potential of the working electrode at various sites within the crevice. Each reference electrode and the working electrode are assigned relay channels. When a potential measurement is taken, all relays are open except those of the reference electrode to be used and the working electrode. This process is repeated for each of the interior reference electrodes. The potential is measured by a Keithley 197A multimeter. The voltmeter has an analog output voltage that

corresponds to the digits displayed on the meter. The ADCB receives this voltage and records it for each electrode. Conversion of the recorded voltage to the actual voltage is performed by the BASIC program using user input of the range setting on the meter. After conversion of analog meter output to digital data all values are stored in a data file. The reference electrode external to the crevice is positioned at the outer edge of the outer ring. The potential difference between this reference electrode and the outer ring is measured by making the voltage measurement directly with the ADCB. A separate channel is employed for this measurement.

The pH at three locations inside the crevice and in the external bulk solution are measured and recorded in a data file. The signals from the pH microelectrodes are amplified using millivolt adapters™ (Microelectrodes, Inc.) before being routed to the relay board. Each electrode is assigned two relays, one for its internal reference and one for its measuring electrode. When a pH measurement is made the BASIC program switches on the two relays corresponding to a given probe. The voltage generated by the probe is measured by the voltmeter and recorded in the same manner as the voltages described above. All pH probes are calibrated against buffers and their voltage outputs are recorded. The recorded voltages are used to convert the voltage data generated by the pH probes back into actual pH values.

Current is measured using a picoammeter. The picoammeter has an inverting analog output which provides a voltage indicating the current LED values for the meter. Conversion of the recorded voltage to the corresponding current is performed by the BASIC program using user input of the range setting on the meter. After conversion to

digital data all values are stored in a data file. Current data is allocated a separate channel on the ADCB.

CHEMICAL AND ELECTROCHEMICAL CONDITIONS IN THE CREVICE ENVIRONMENT

The onset of MIC typically involves the development of oxygen concentration cells between the area under the crevice and the surrounding outer surface, with the area under the crevice becoming anodic and the remaining surface serving as the cathodic site. This results in localized attack of the metal in the crevice for various reasons:[11]

(1) the ratio of anode area to cathode area
(2) differential aeration
(3) pH changes at the anode and cathode
(4) formation of corrosion products.

Consider a carbon steel sample placed in a 3.5 weight % solution of NaCl in H_2O. An artificial crevice is formed on the steel by a piece of Plexiglas. Initially, the oxidation of iron and the reduction of oxygen occur uniformly over the entire steel sample by the reactions:

$$Fe \rightarrow Fe^{2+} + 2e^- \quad (9)$$

$$O_2 + 2H_2O + 4e^- \rightarrow 4OH^- \quad (10)$$

After a short period of time, the oxygen reduction reaction ceases to occur in the crevice due to the restricted convection of oxygen into the crevice. Thus, the only reaction now occurring inside the crevice is iron dissolution.

The production of Fe^{2+} ions in the crevice causes an excess of positive charge in this area, which is balanced by the migration of Cl^- ions to the anodic site. If it is assumed

that the iron hydroxide is the thermodynamically stable phase in this solution, the Fe^{2+} ions will be hydrolyzed by water through the reactions:

$$Fe^{2+} + 2H_2O \rightarrow Fe(OH)_2 + 2H^+ \quad (11)$$
$$3Fe^{3+} + 3H_2O \rightarrow Fe(OH)_3 + 3H^+ \quad (12)$$

It can therefore be seen that the presence of Cl^- and H^+ ions in the crevice results in the production of acidic hydrochloric acid, HCl, further aiding the localized attack in the crevice. It can also be seen that the pH in the crevice environment decreases where the pH of the outer surface, where oxygen reduction occurs, increases.

Leidheiser and co-workers[12] found that the pH inside a 0.032 cm crevice on 1018 carbon steel in 3.5% NaCl is alkaline upon initial exposure to the solution, in the range of 10-12. After 100 hours, the pH fell to the neutral-to-slightly acidic range, about 6-7. Pourbaix and Van Muylder[13] observed a crevice pH in the range of 2.7 to 4.7 with an outer surface pH of about 10. Pickering and Frankenthal[14] theorized that the concentration of Cl^- and Fe^{2+} increases as you go further into a pit or crevice, since iron dissolution occurs at the bottom of the pit or crevice and chloride ions migrate to anodic sites. The concentration of H^+ decreases as you go further into a crevice due to the tendency for cations to move away from the anode. The potential ϕ of the electrolyte, which is defined as the difference in the potential at the outer surface and the potential at some distance within the crevice,

$$\phi = E_{x=0} - E_x \quad (13)$$

increases with increasing distance into the crevice, meaning that the potential of the metal within the crevice gets increasingly negative.

THERMODYNAMIC CONDITIONS IN THE CREVICE ENVIRONMENT

An examination of the Potential-pH diagram for the iron-sodium-chlorine-water system in Figures 3a-d reveals the regions of thermodynamic immunity, passivity, and active corrosion for varying activities of Fe^{2+}. The region of thermodynamic stability of the species Fe represents the region of immunity, that of Fe^{2+} represents the region of active corrosion, and those of oxides and hydroxides represent the regions of passivity. The equilibrium lines between Fe and Fe^{2+}, Fe_2O_3 and Fe^{2+}, and Fe_3O_4 and Fe^{2+} shift with change in the activity of Fe^{2+}, $a_{Fe}{}^{2+}$, which is produced when iron corrodes. Thus, by knowing the pH, potential, and activity of Fe^{2+} (which is a function of the concentration of Fe^{2+}) in the crevice environment, it can be predicted whether the metal in the crevice is immune, passive, or actively corroding.

Metastable passive films may exist in the region of assumed active corrosion. The term *metastable* refers to films that are not as stable as they would be if they were in their respective regions of thermodynamic stability, as determined by the Pourbaix diagram. These films can be identified on the diagram by extrapolating the equilibrium lines between Fe_3O_4 & Fe and Fe_3O_4 & Fe_2O_3 into the region of Fe^{2+}. Within these bounding lines, metastable passivity is possible, and this phenomenon may account for corrosion rates that are lower than expected.

The thermodynamic conditions necessary in the crevice for cathodic protection to be effective may also be predicted from the Potential-pH diagram. A similar analysis of the iron-sodium-chlorine-sulfur-water Pourbaix diagram as in Figures 4a-d will lead to the

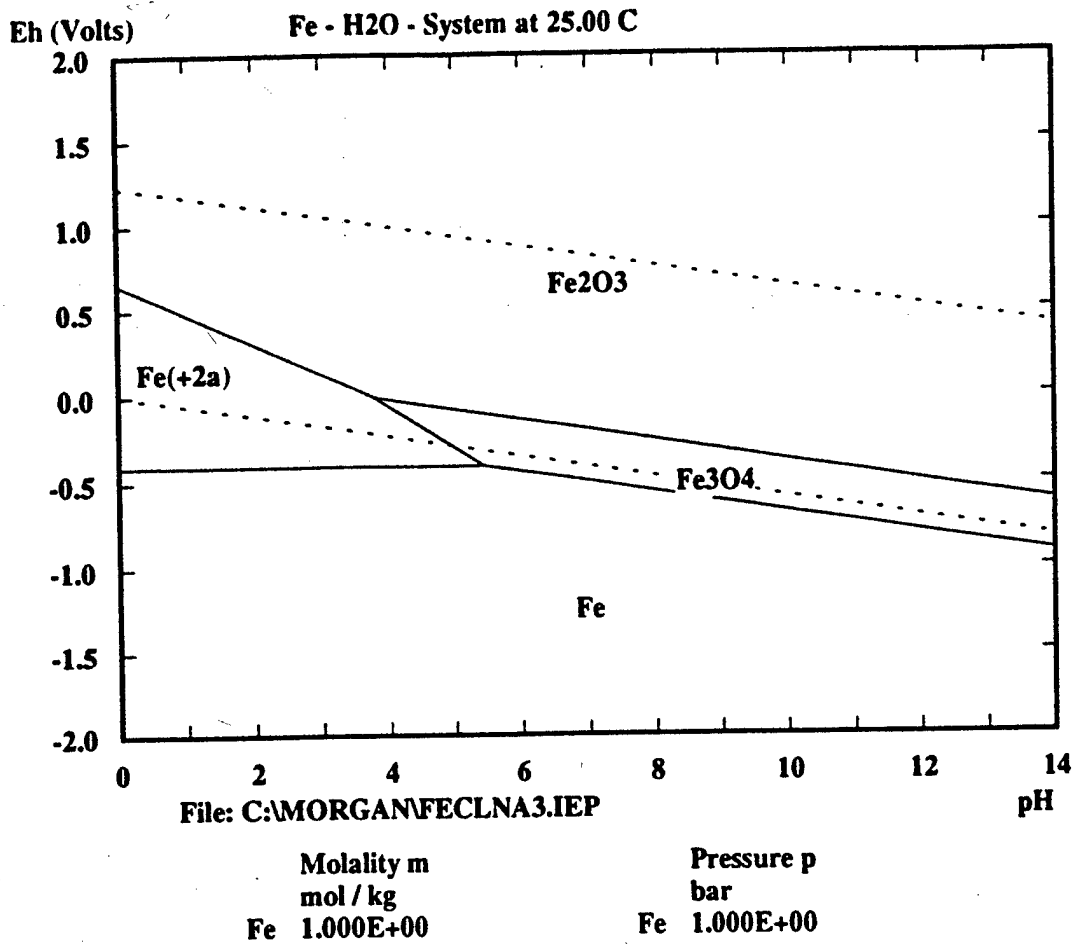

Figure 3a: Potential-pH diagram for the Fe-Cl-Na-H_2O system for an activity of Fe^{2+} of 1.000E+00.

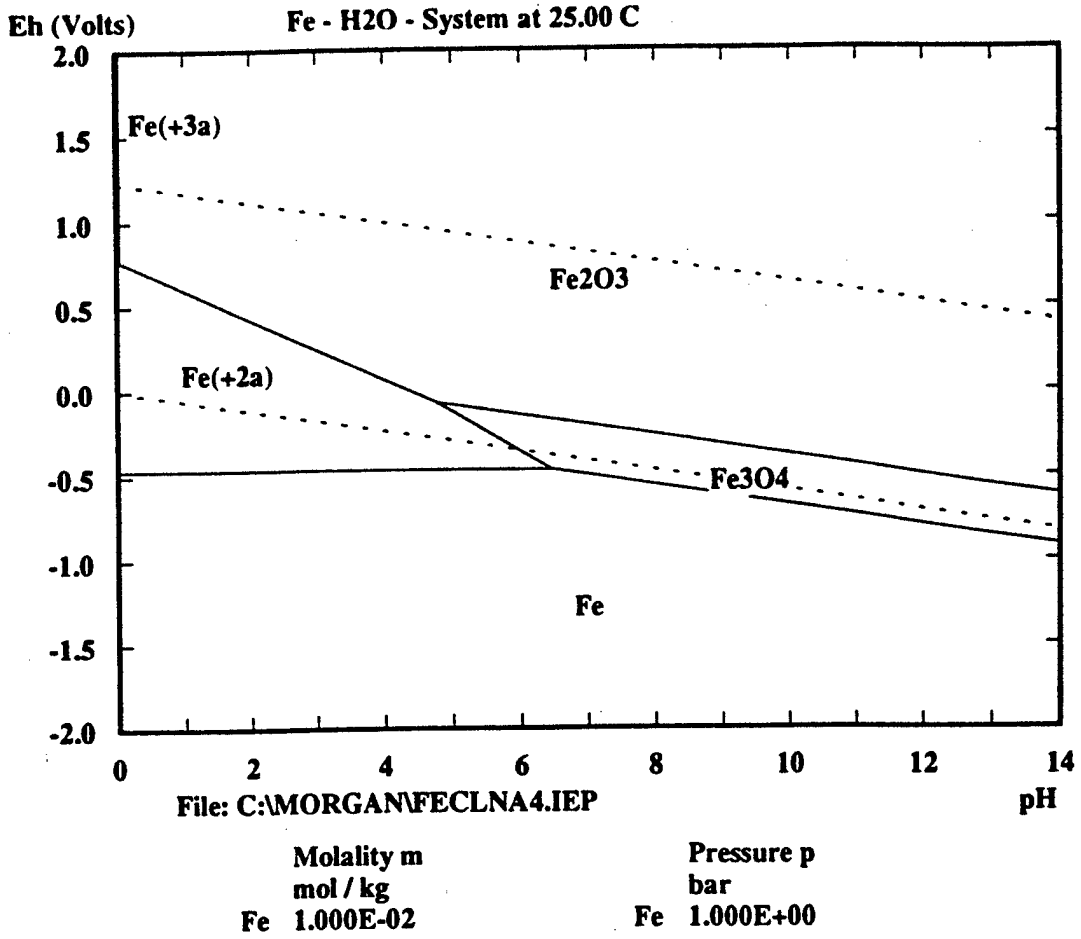

Figure 3b: Potential-pH diagram for the Fe-Cl-Na-H_2O system for an activity of Fe^{2+} of 1.000E-02.

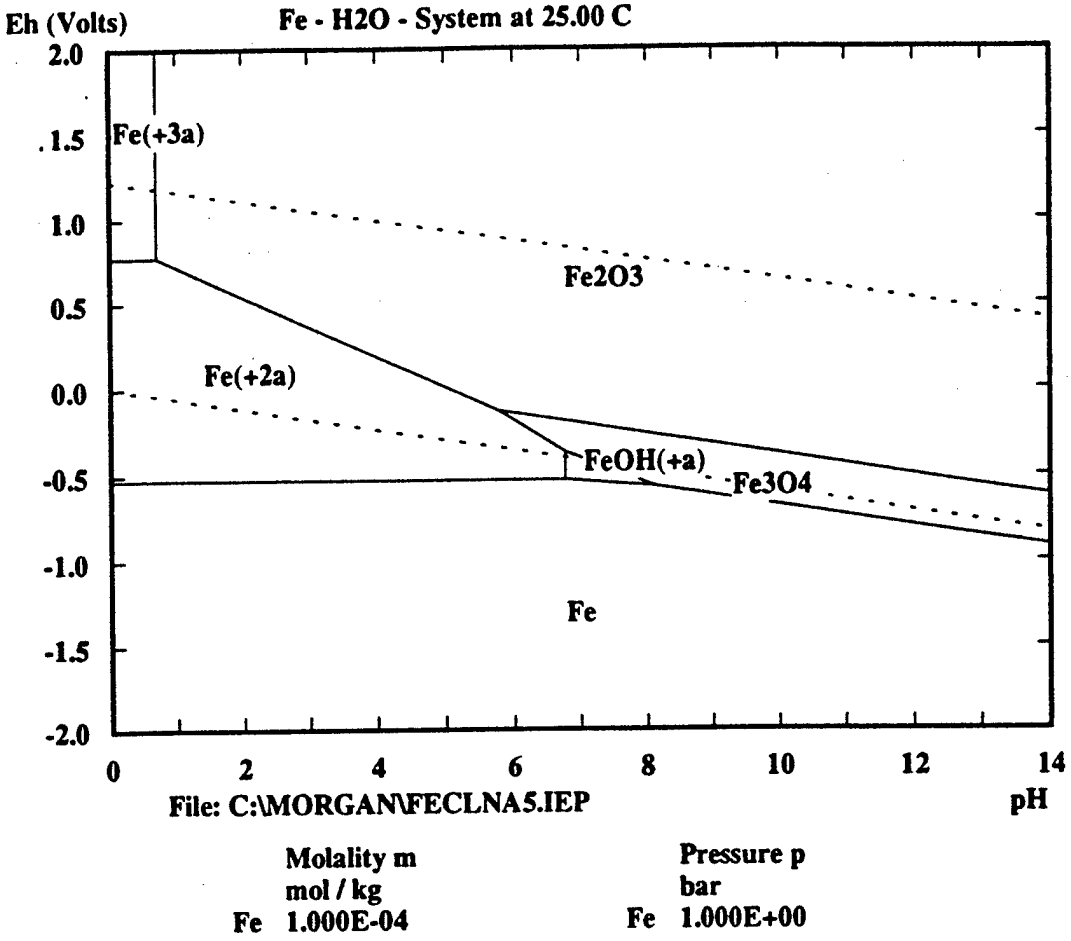

Figure 3c: Potential-pH diagram for the Fe-Cl-Na-H_2O system for an activity of Fe^{2+} of 1.000E-04.

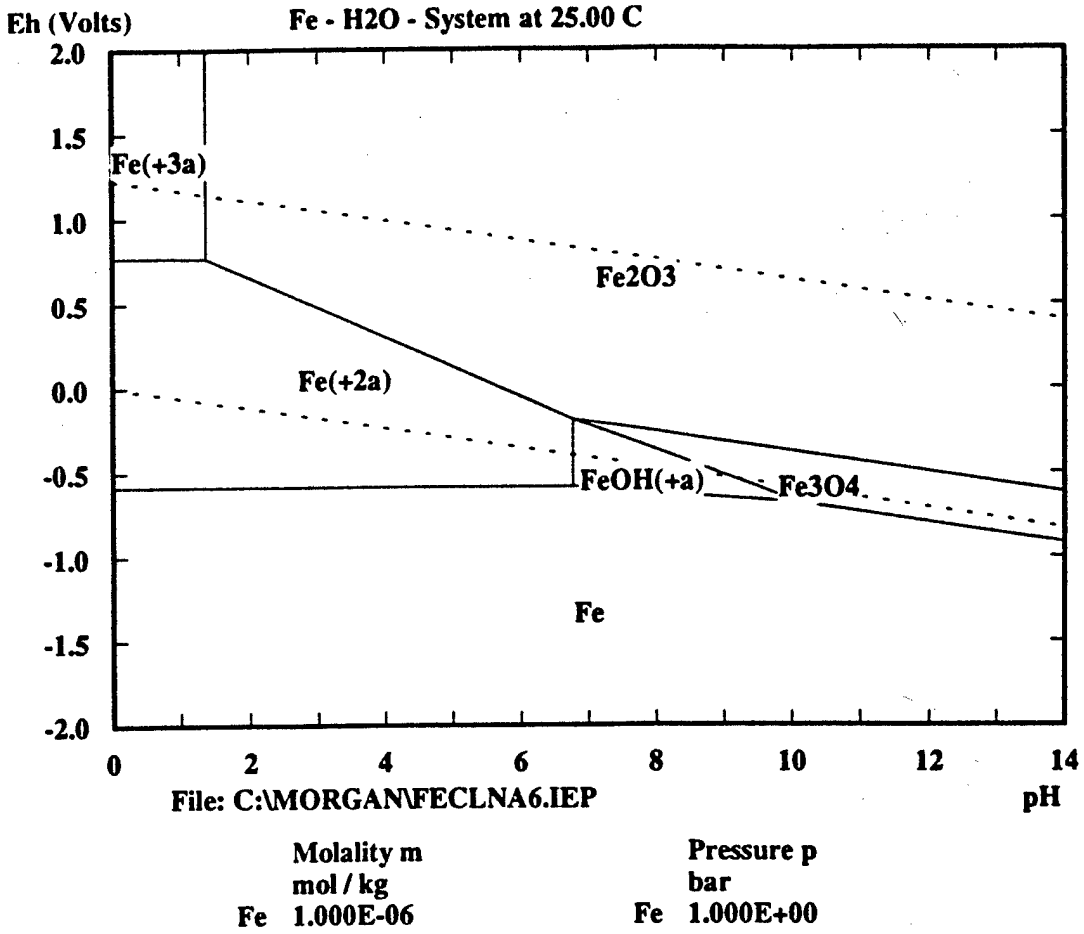

Figure 3d: Potential-pH diagram for the Fe-Cl-Na-H_2O system for an activity of Fe^{2+} of 1.000E-06.

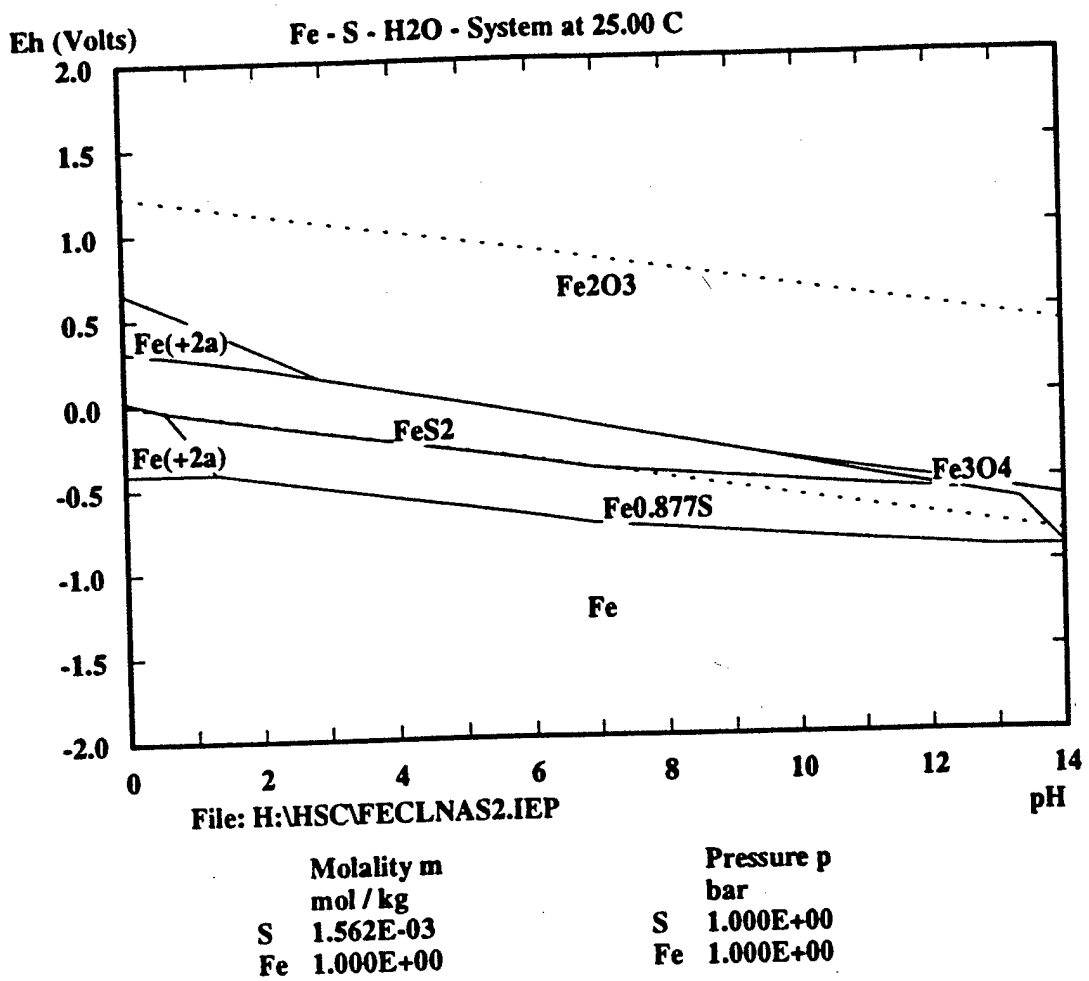

Figure 4a: Potential-pH diagram for the Fe-Cl-Na-S-H_2O system for an activity of Fe^{2+} of 1.000E+00.

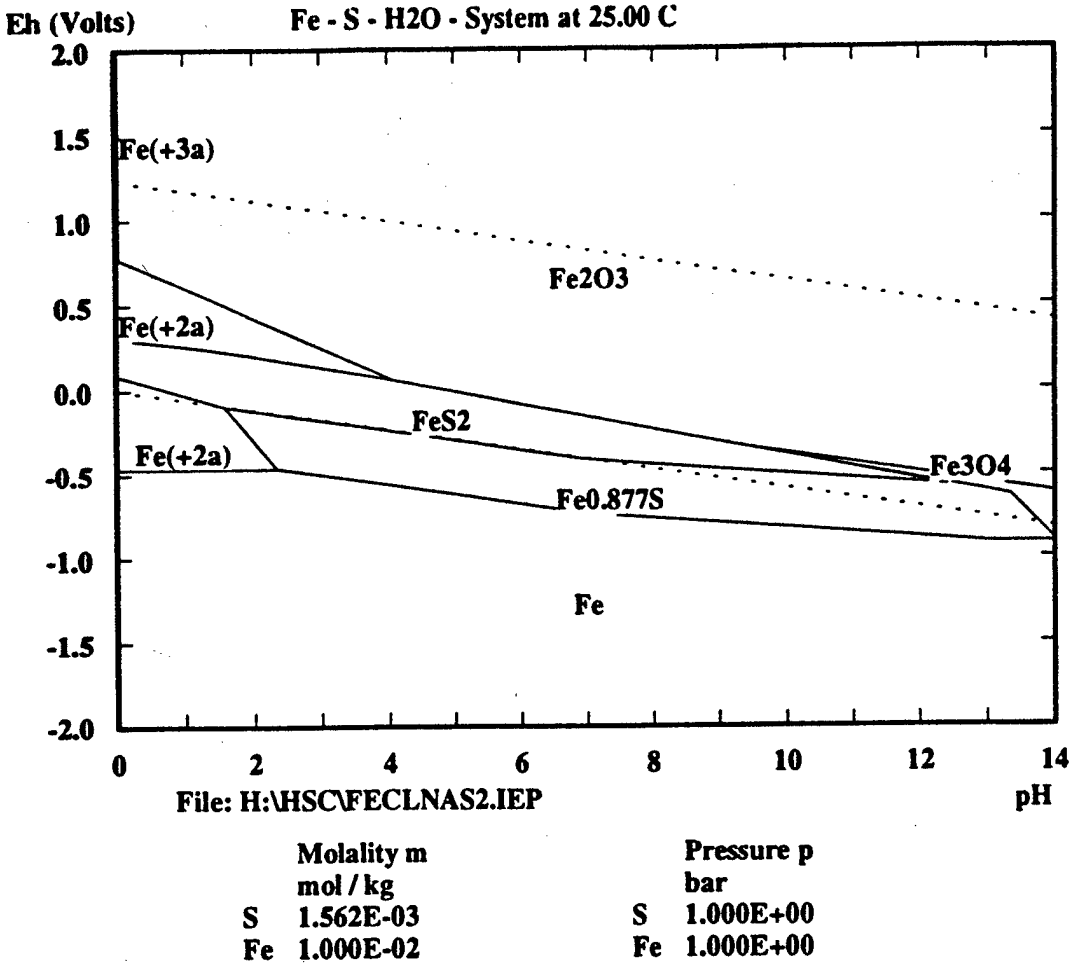

Figure 4b: Potential-pH diagram for the Fe-Cl-Na-S-H_2O system for an activity of Fe^{2+} of 1.000E-02.

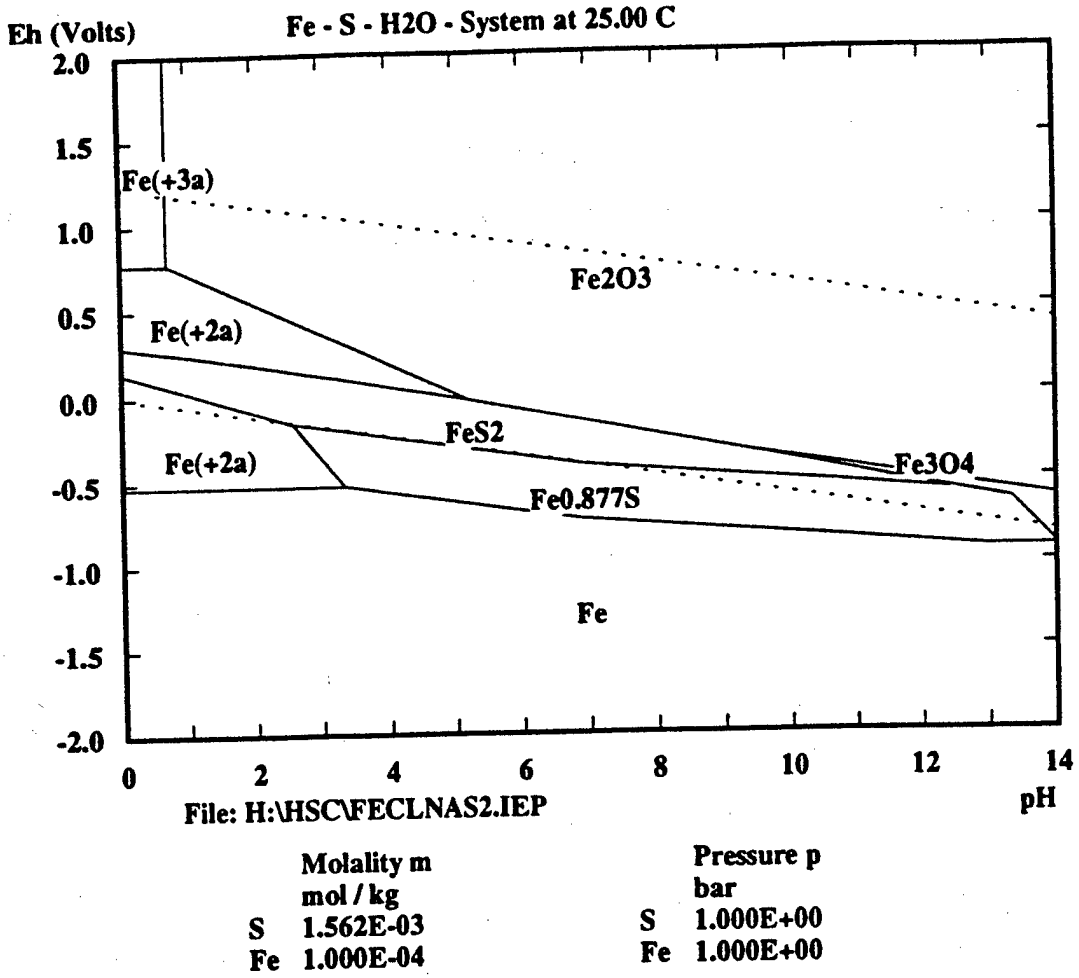

Figure 4c: Potential-pH diagram for the Fe-Cl-Na-S-H_2O system for an activity of Fe^{2+} of 1.000E-04.

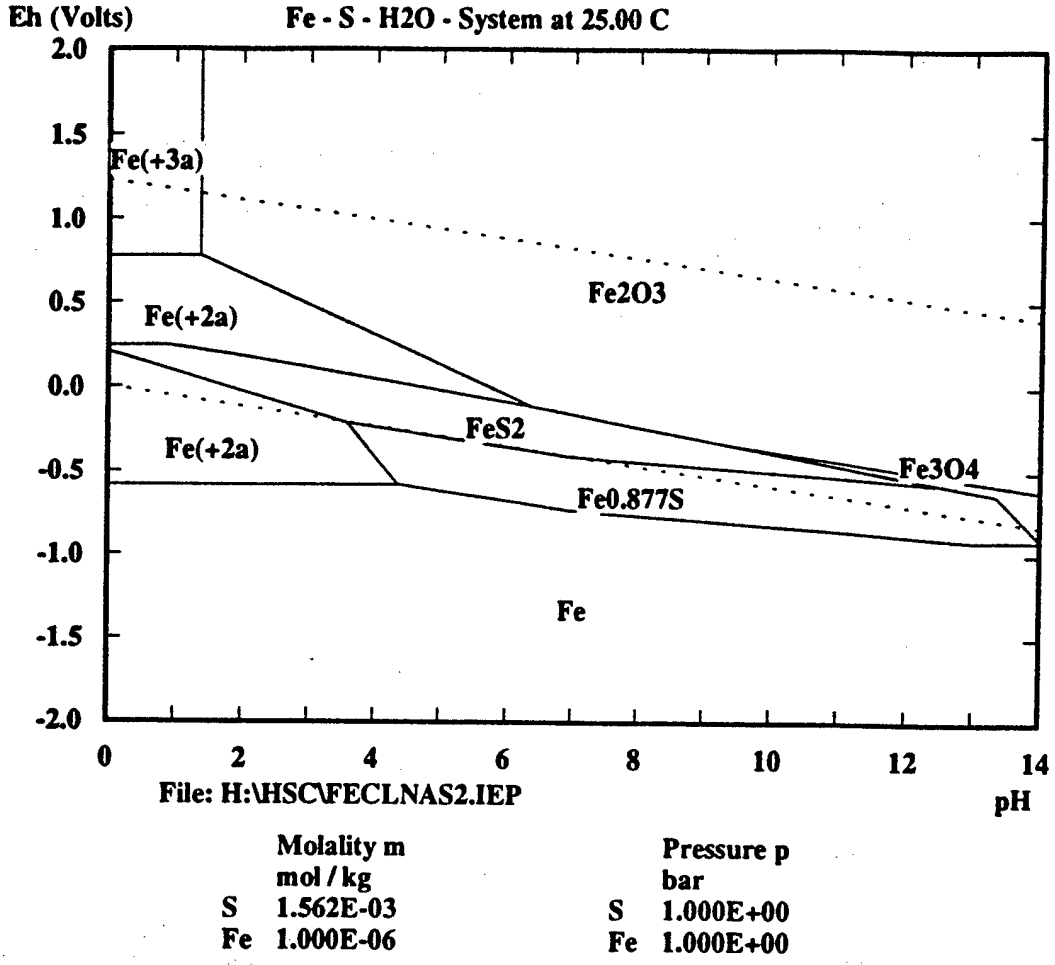

Figure 4d: Potential-pH diagram for the Fe-Cl-Na-S-H_2O system for an activity of Fe^{2+} of 1.000E-06.

thermodynamic conditions necessary for adequate cathodic protection of carbon steel in the presence of SRB.

Results

The Plexiglas crevice former is arrayed with three sets of holes, consisting of five holes each. In this fashion, a number of data points can be established for each of five distances from the center of the crevice. Since our design employs radial symmetry, the center of the crevice can essentially be viewed as the "bottom" of the crevice. Thus, data points for pH and potential measurements were taken at distances of 3.8, 13.4, and 23.1 mm from the crevice center and were labeled 1, 3, and 5, respectively. The sets of points from which these holes came were labeled B, G, and R, and will be used to distinguish each individual hole. For example, the hole in set B at 3.8 mm from the center is labeled B1. See Figure 2.

Electric leads soldered onto the crevice disk and the outer ring were connected to a zero resistance ammeter and current was monitored between the creviced disk and the outer ring during open circuit crevice corrosion, as can be seen in Figure 5. The creviced sample in seawater without sulfides turned anodic relative to the outer ring, that is, the current value on the ammeter became positive, after 2 hr, 40 min. The creviced sample in the seawater with injected sulfides turned anodic almost an hour earlier, after 1 hr, 50 min. The creviced sample with the agarose film on it turned anodic after 2 hr, 20 min., faster than in plain seawater, but not as fast as with the sulfides. The experiments with the sulfides produced the greatest amount of current (approximately 83 μA), with the experiments involving plain seawater and seawater with the agarose film having about the

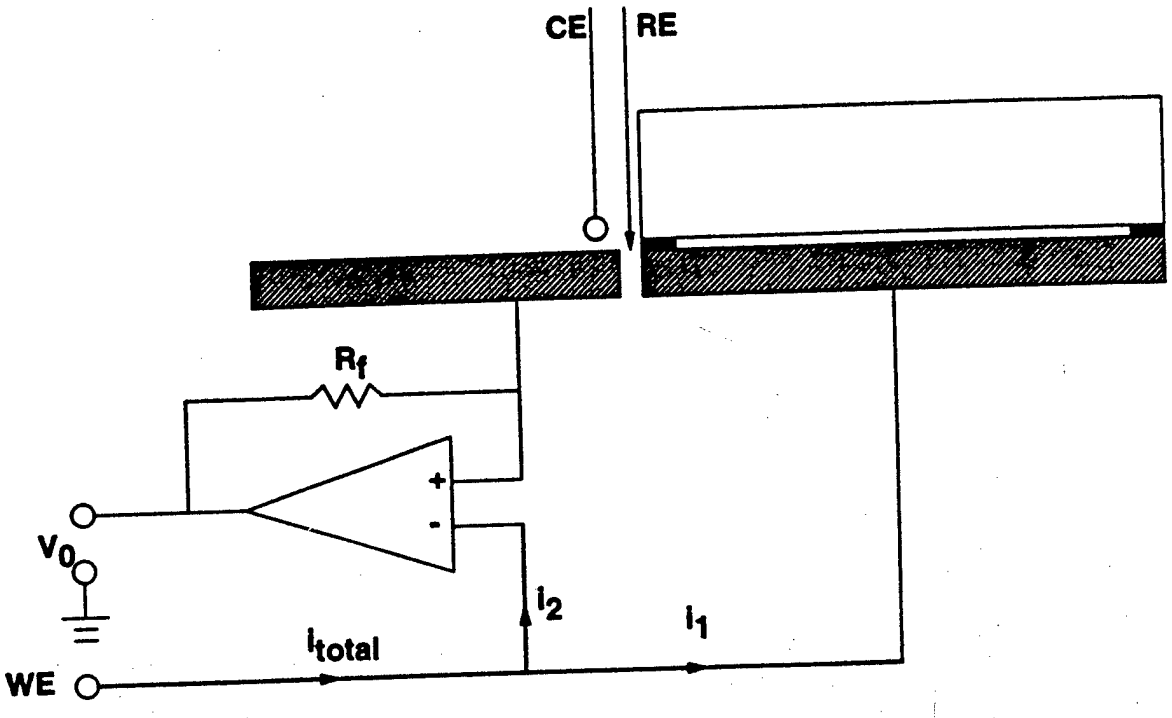

Figure 5: Circuit for Zero Resistance Ammeter

same amount of current emanating from the crevice, differing by only 5 μA (4 - 9 μA). This is due to the acceleration of corrosion by the sulfides and the production of an iron sulfide film.

An examination of the open circuit potential measured by the reference electrode at the crevice mouth, shown in Figure 6, shows a decrease of about 35 mV (from -0.725 to -0.760 V vs. SCE) after 24 hours when sulfides are introduced into the system. Each experiment showed a gradual decrease in open circuit potential with time, starting in the region of -0.44 to -0.55 V vs. SCE upon initial exposure to electrolyte.

A series of Luggin capillaries with agar salt bridges were used in conjunction with Saturated Calomel Electrodes to measure potential at different depths inside the crevice. Each and every one of the measurement points for each experiment displayed a decrease in the potential of the carbon steel inside the crevice with time, as shown in Figures 7, 8, and 9.

The potential decreased slightly with increasing distance into the crevice for each of the sets of holes, with the exception of the experiments involving sulfides, which showed virtually no change in values between points. The potential was essentially constant for all experiments, with maximum changes of only 1-2 mV. See Figures 7, 8, and 9.

pH measurements were taken with Ag/AgCl pH/reference combination microelectrodes. Figures 10 and 11 show a general trend of decreasing pH with time for each of the measurement points. However, Figure 12 shows an *increasing* pH with time when sulfides are in the system.

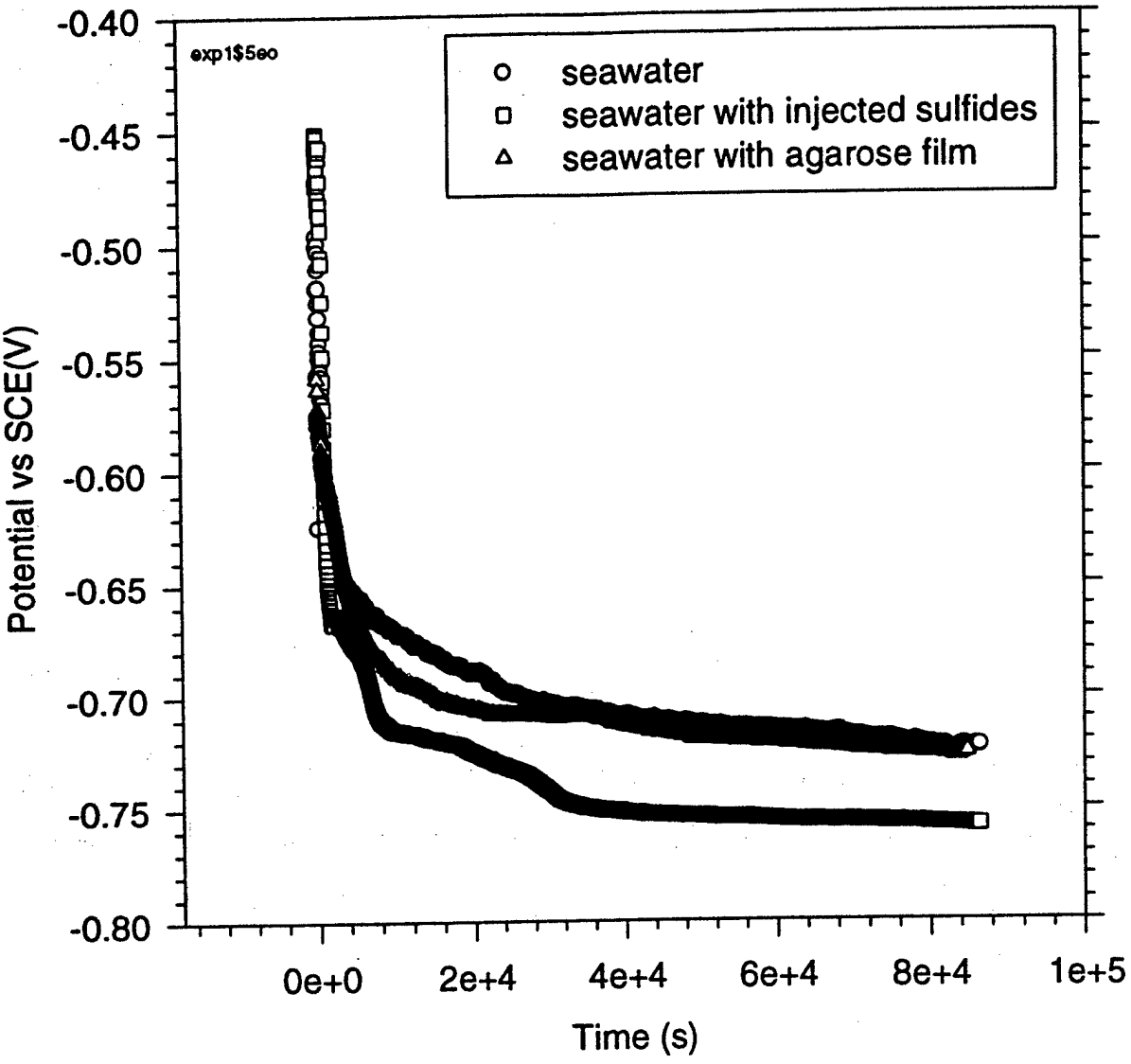

Figure 6: Potential (V vs. SCE) vs. Time (s) for open circuit crevice corrosion in 3.5 wt.% seawater as measured at the crevice mouth.

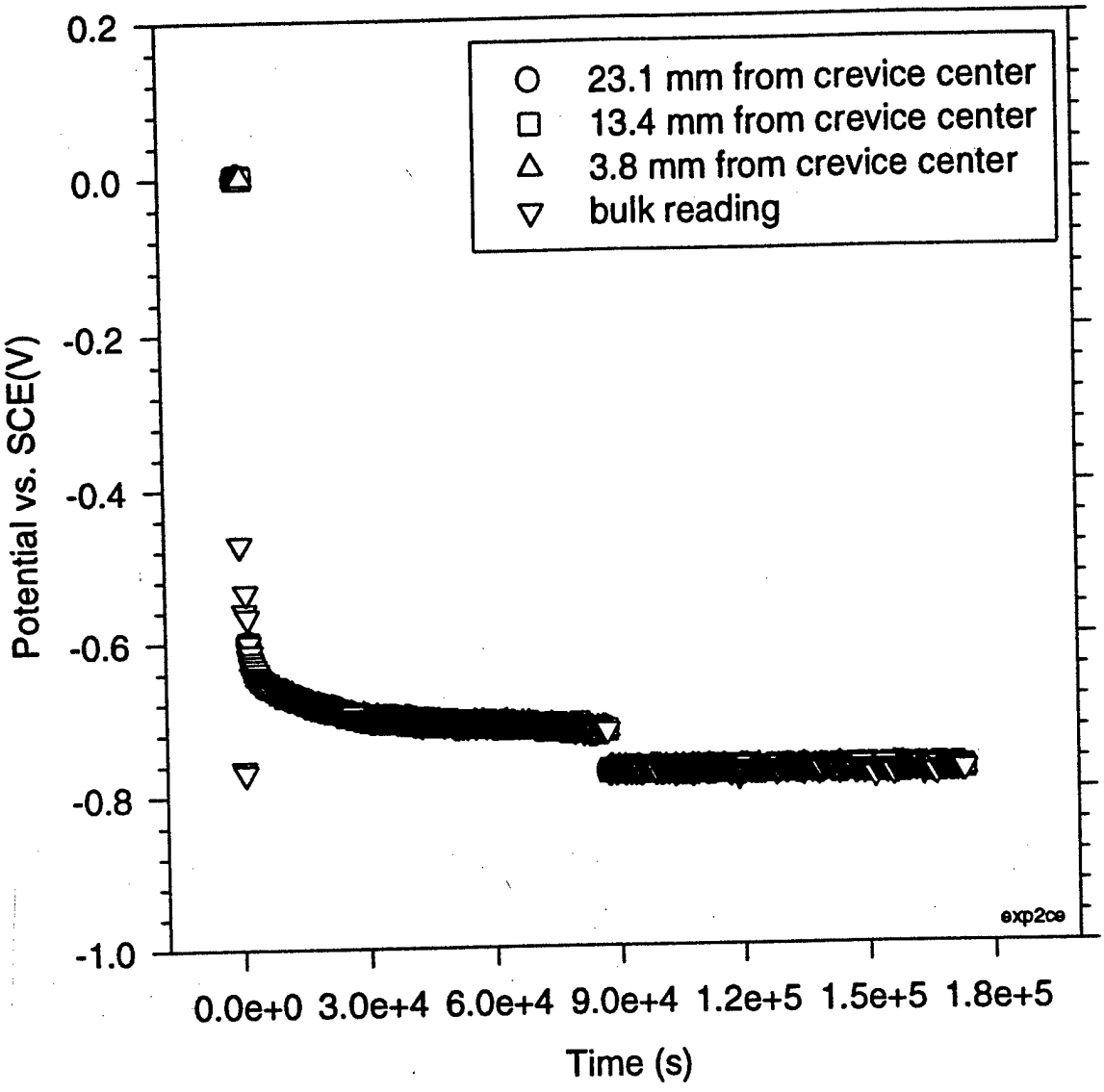

Figure 7: Potential (V vs. SCE) vs. Time (s) for open circuit and cathodic protection in 3.5 wt.% seawater.

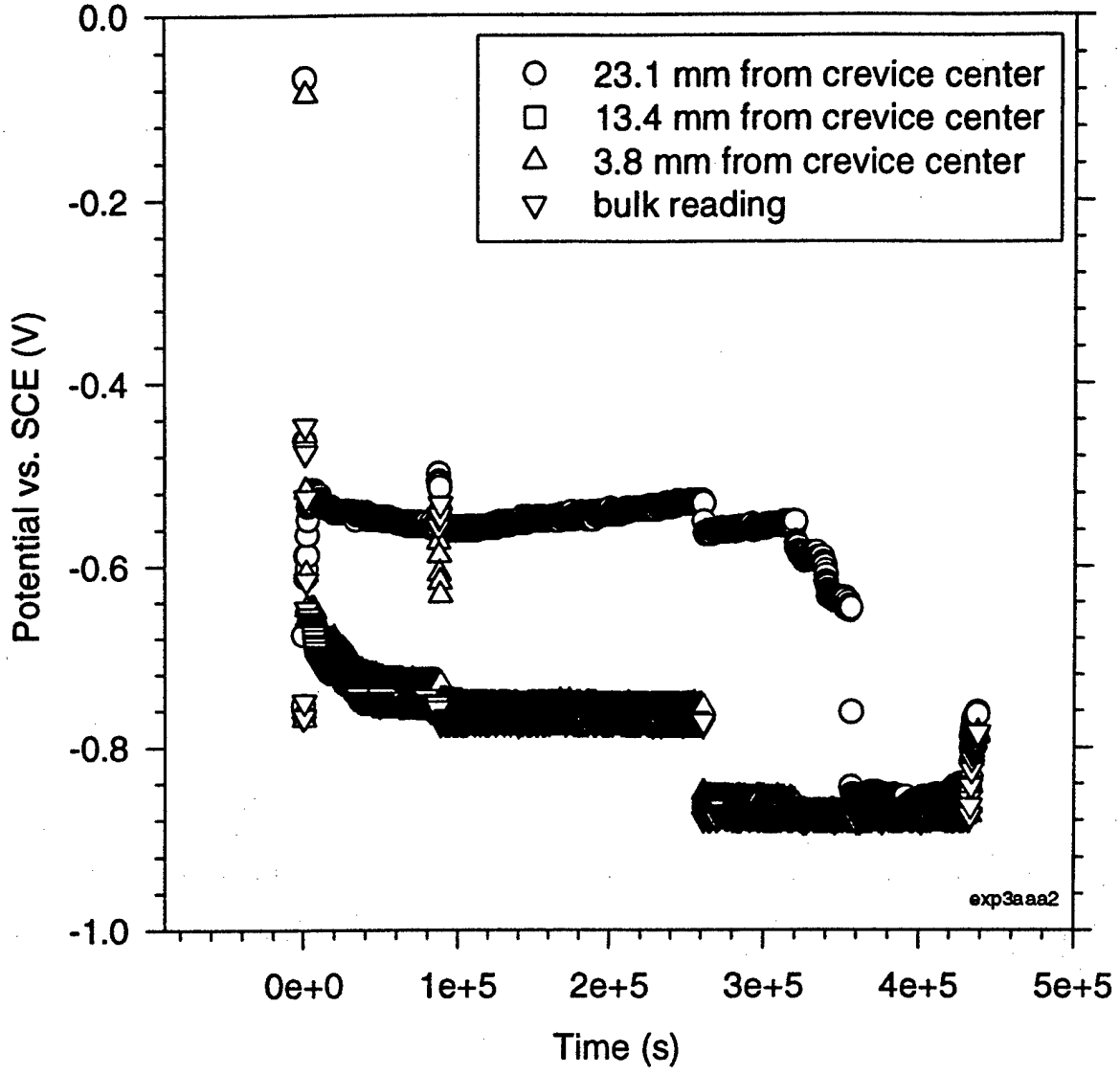

Figure 8: Potential (V vs. SCE) vs. Time (s) for open circuit and cathodic protection in 3.5 wt.% seawater with injected sulfides.

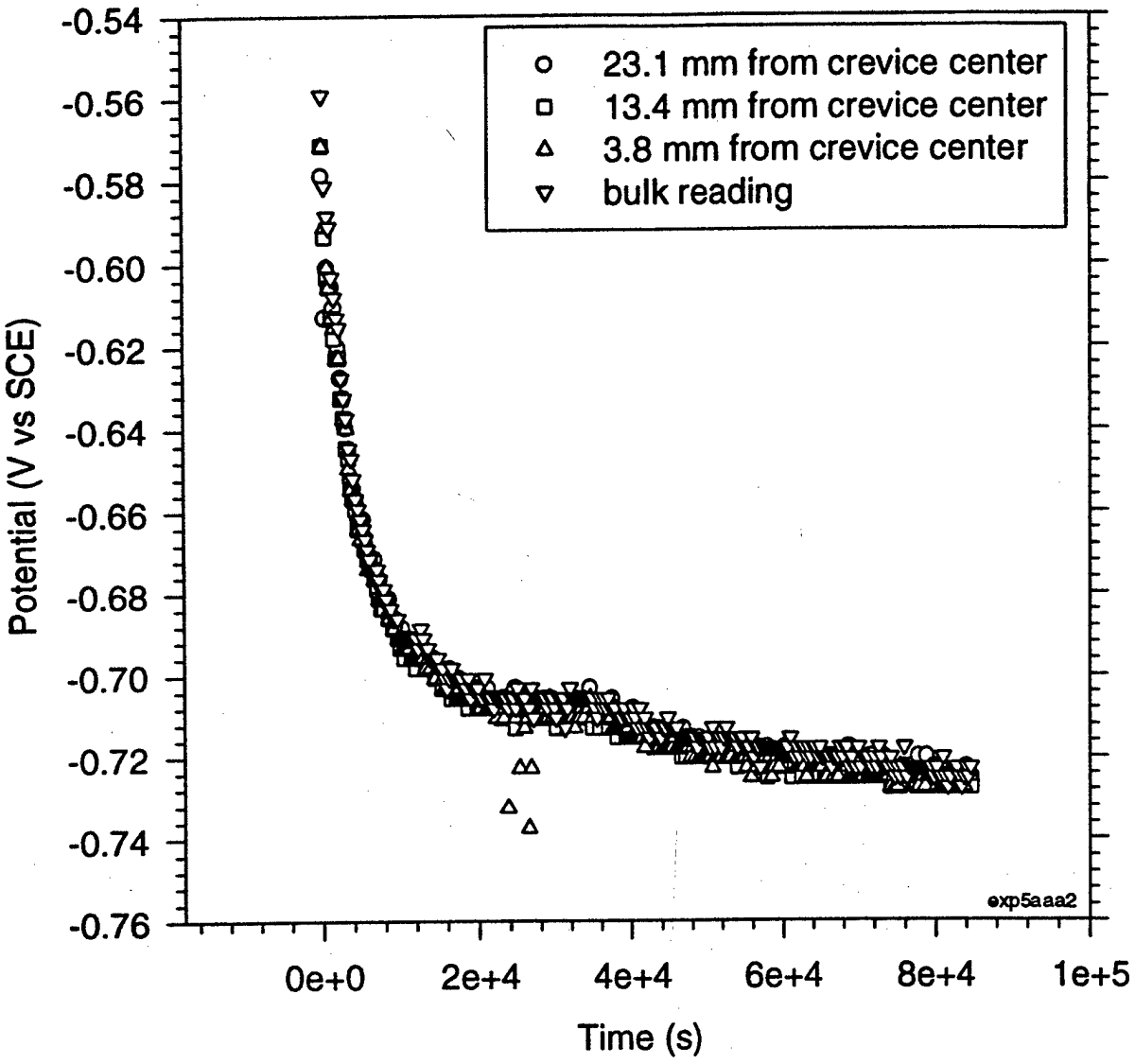

Figure 9: Potential (V vs. SCE) vs. Time (s) for open circuit and cathodic protection in 3.5 wt.% seawater with an agarose film.

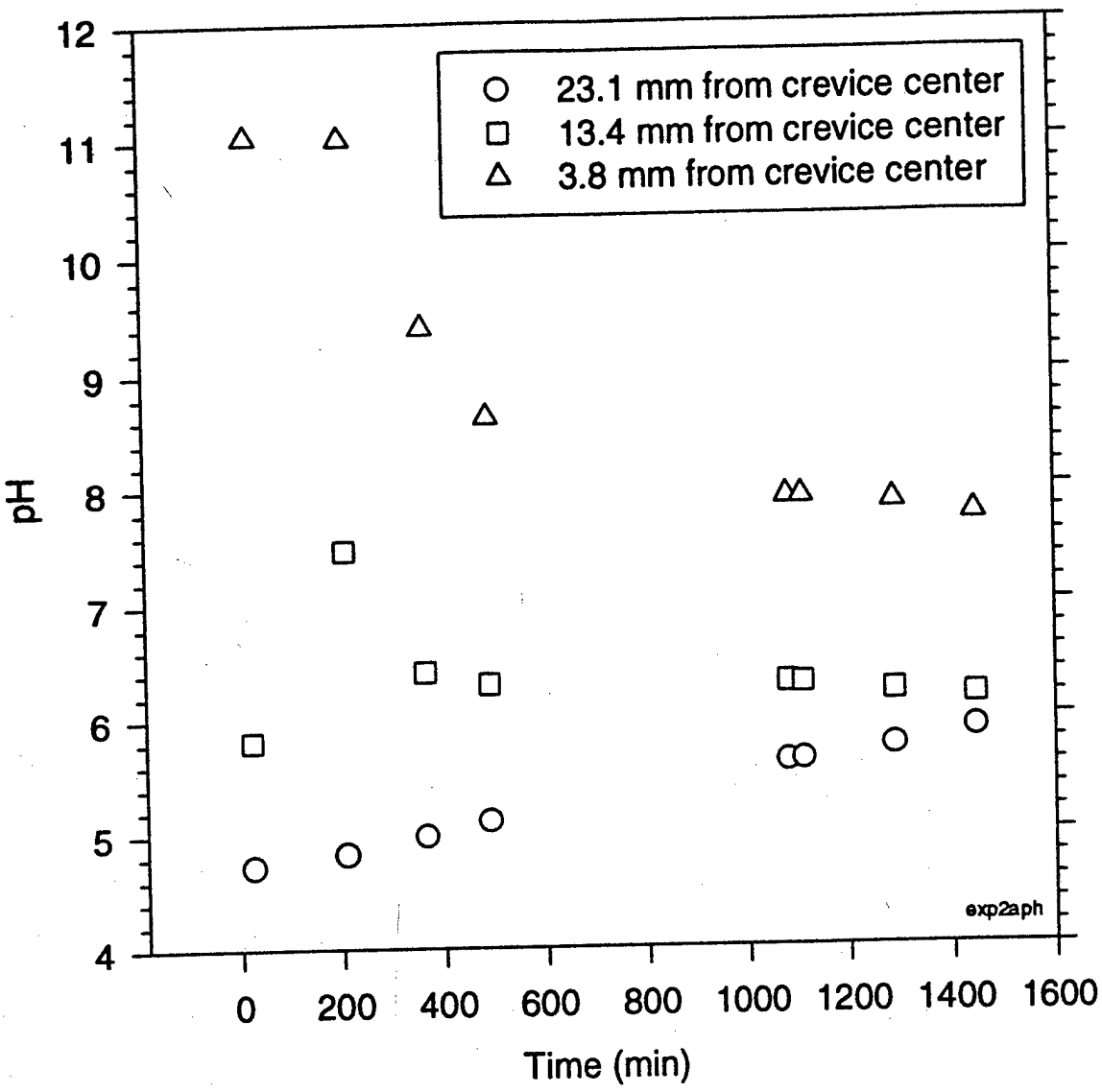

Figure 10: pH vs. Time (min) during open circuit crevice corrosion in 3.5 wt.% seawater.

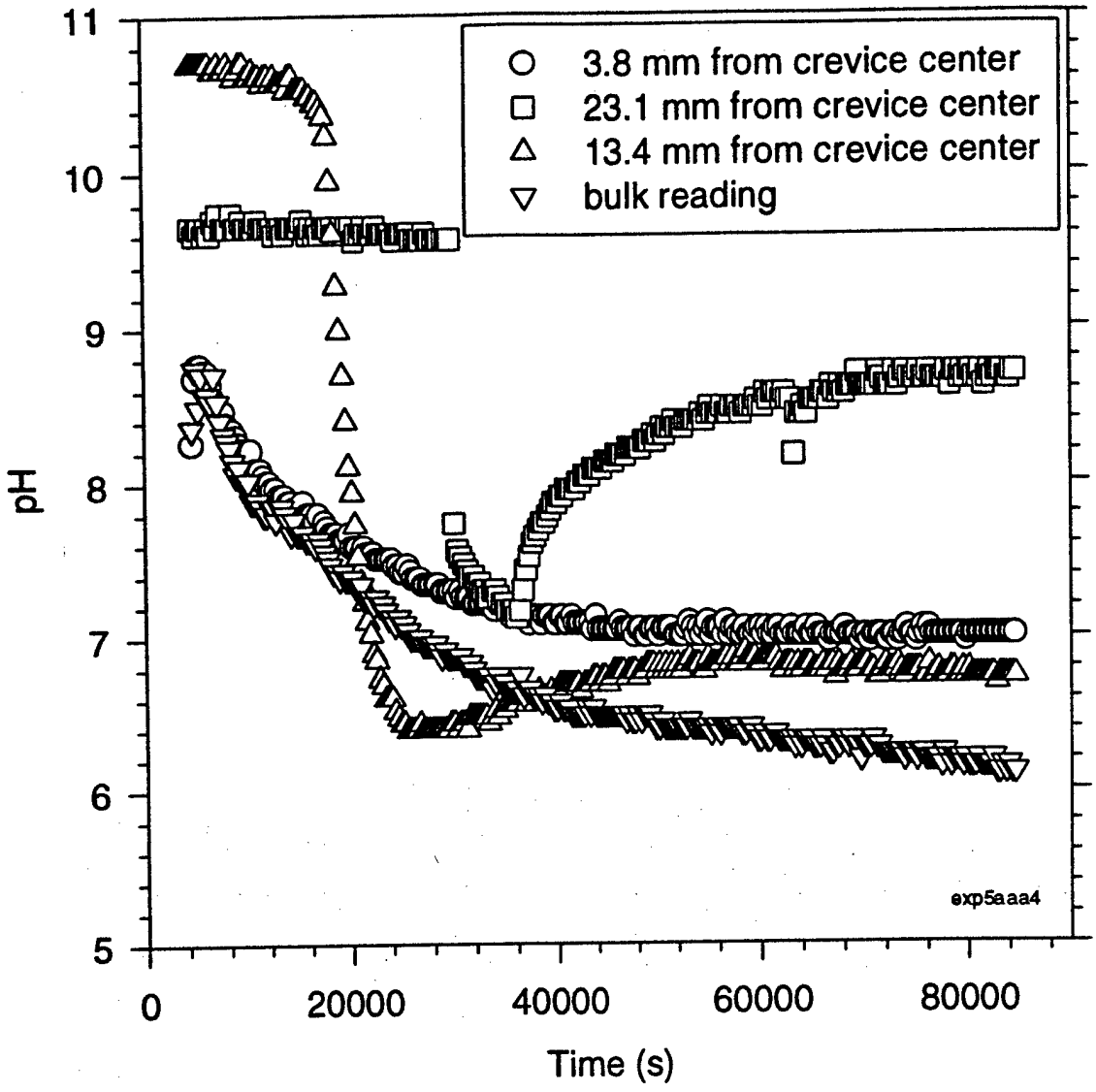

Figure 11: pH vs. Time (s) during open circuit crevice corrosion in 3.5 wt.% seawater with an agarose film.

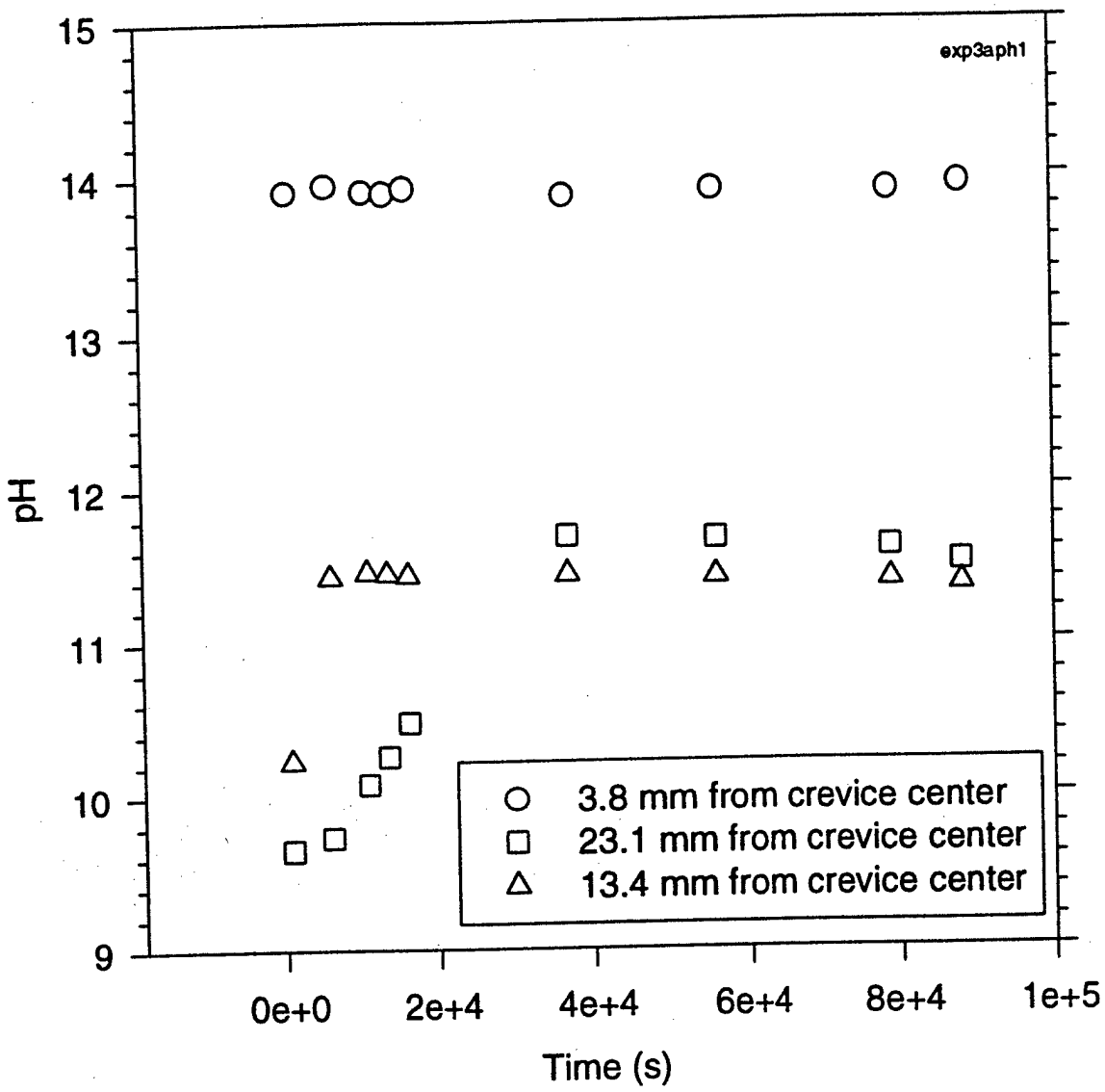

Figure 12: pH vs. Time (s) during open circuit crevice corrosion in 3.5 wt.% seawater with injected sulfides.

With increasing distance into the crevice, the pH increased for each set of points during the crevicing experiments with and without sulfides. However, when agarose was introduced, a decrease in pH with increasing distance into the crevice was observed. The experiments in seawater without sulfides and those with agarose showed pH values ranging from slightly acidic to near neutral. When sulfides were involved, pH values were considerably higher and alkaline.

Discussion

Much of the data accumulated in the open circuit experiments point to the development of a crevice environment: anodic current flowing from the crevice, decrease in pH from basic to slightly acidic/near neutral values, and a potential drop. The initial decrease in current upon initiation of the experiment showed the outer ring was predominantly the anode, as both iron dissolution and oxygen reduction were occurring on both the creviced steel and the outer ring. The larger surface area of the outer ring may have been influential in this regard. Once the oxygen in the crevice was depleted, the current began to rise until it became a positive value, at which point, the creviced steel became the anode due to the fact that the crevice restricted migration of oxygen into the crevice area and allowed only for iron dissolution.

The decrease in pH with time inside the crevice for the simulated seawater crevicing experiments without sulfides and with agarose can be accounted for by the hydrolysis reaction, reactions # 11 and 12. The production of H^+ ions drove the pH down

inside the crevice. The increase in pH over time for the experiments involving sulfides can be explained by the following set of reactions:

$$Na_2S \rightarrow 2Na^{2+} + S^{2-} \quad (14)$$

$$H_2O + S^{2-} \rightarrow HS^- + OH^- \quad (15)$$

$$HS^- + H_2O \rightarrow H_2S_{(aq)} + OH^- \quad (16)$$

Or

$$H^+ + S^{2-} \rightarrow HS^- \quad (17)$$

$$H^+ + HS^- \rightarrow H_2S \quad (18)$$

Figures 10 and 11 show that the trend is for the pH to increase into the crevice, since the H^+ ions migrate away from the anodic site. For the experiments with agarose, however, with increasing time, the trend was for the pH to *decrease* into the crevice, perhaps due to the production of H^+ ions in the hydrolysis reaction, the production of iron sulfide by the reaction:

$$Fe^{2+} + HS^- \rightarrow FeS + H^+ \quad (19)$$

and/or the migration of Cl^- ions to the anode, leading to the production of HCl in the crevice. Even in the simple crevicing experiments with and without sulfides, the *degree* of pH increase going into the crevice reduced considerably over time.

Figures 7, 8, and 9 show that the decrease in potential in the crevice seems to level off at a value of approximately -0.725 to -0.730 V vs. SCE for each of the data points in the absence of sulfides, and -0.760 V vs. SCE in the presence of sulfides. The gradual decrease in open circuit potential as measured by the reference electrode at the crevice mouth can be explained by the transformation of the air-formed oxide film on the steel surface upon initial exposure to an electrical double layer. The decreasing potential trend

is a result of the formation of a porous hydroxide layer that only slows the rate of corrosion, but does not protect the metal from further corrosion. The corresponding pH values at this time were slightly acidic to near neutral in the absence of sulfides and rather basic in the presence of sulfides. From Figures 3a-d it can be seen that at the values for carbon steel crevice corrosion without sulfides, both iron dissolution and the hydrolysis reaction are thermodynamically possible. This adds further support for the development of a crevice environment, with an ever decreasing potential from the dissolution of iron, an increase in H^+ concentration and a decrease in Fe^{2+} concentration from the hydrolysis reaction. When sulfides are present, the values for carbon steel crevice corrosion indicate the thermodynamic stability of either an FeS film or a hydroxide film, both rather unprotective, as can be seen from Figures 4a-d.

The potential decreased with distance into the crevice. Values were relatively constant in the crevice during active crevice corrosion, with increases or decreases of no more than 1-2 mV. This is indicative of the IR drop mechanism in crevice corrosion, where the outer surface is passive and potential drops off into the crevice, that is, becomes increasingly negative into the crevice, falling into the active corrosion region of the polarization curve.

CATHODIC PROTECTION

Cathodic protection involves the impression of current to a substrate in order to drive it, electrochemically, into a region of thermodynamic immunity. Based on the previous experiments and on relevant literature surveys[10], it is clear that the potential must

be below the equilibrium potential of Fe/Fe^{2+} at minimal concentrations of Fe^{2+} for cathodic protection to be effective. This correlates to an applied potential of -0.7755 V vs. SCE. At this potential, the only thermodynamically possible states in the iron-sodium-chloride-water system are Fe, Fe_3O_4, or $Fe(OH)_2$ depending on the pH, with each state possessing a varying degree of protection. An additional 100 mV of protection is needed to protect carbon steel in the presence of sulfides.

Peterson and Lennox[15] observed pH changes in cathodically polarized creviced samples of stainless steel and copper in 0.6 M NaCl solution. What they observed was a change from near-neutral pH values to basic values in the range 11-12. This increase in pH was rationalized by the consumption of the H^+ ion in the hydrogen evolution reaction.

The ammeter and potentiostat are connected such that current flowing into the crevice *beneath* the simulated tubercle can be indirectly calculated by subtracting the current read on the ammeter (current flowing from the platinum counter electrode to the outer ring) from the current read on the potentiostat (current flowing from the platinum counter electrode to both the outer ring and the inner creviced disk). See the circuit in Figure 5.

Results

The plot of current vs. time for all three types of experiments in Figure 13 shows that under cathodic protection conditions, the current magnitude increases cathodically with time. Almost all protective current was consumed on the outer ring, before it ever reached the mouth of the crevice, as seen in Figures 14-16. The measured potential within

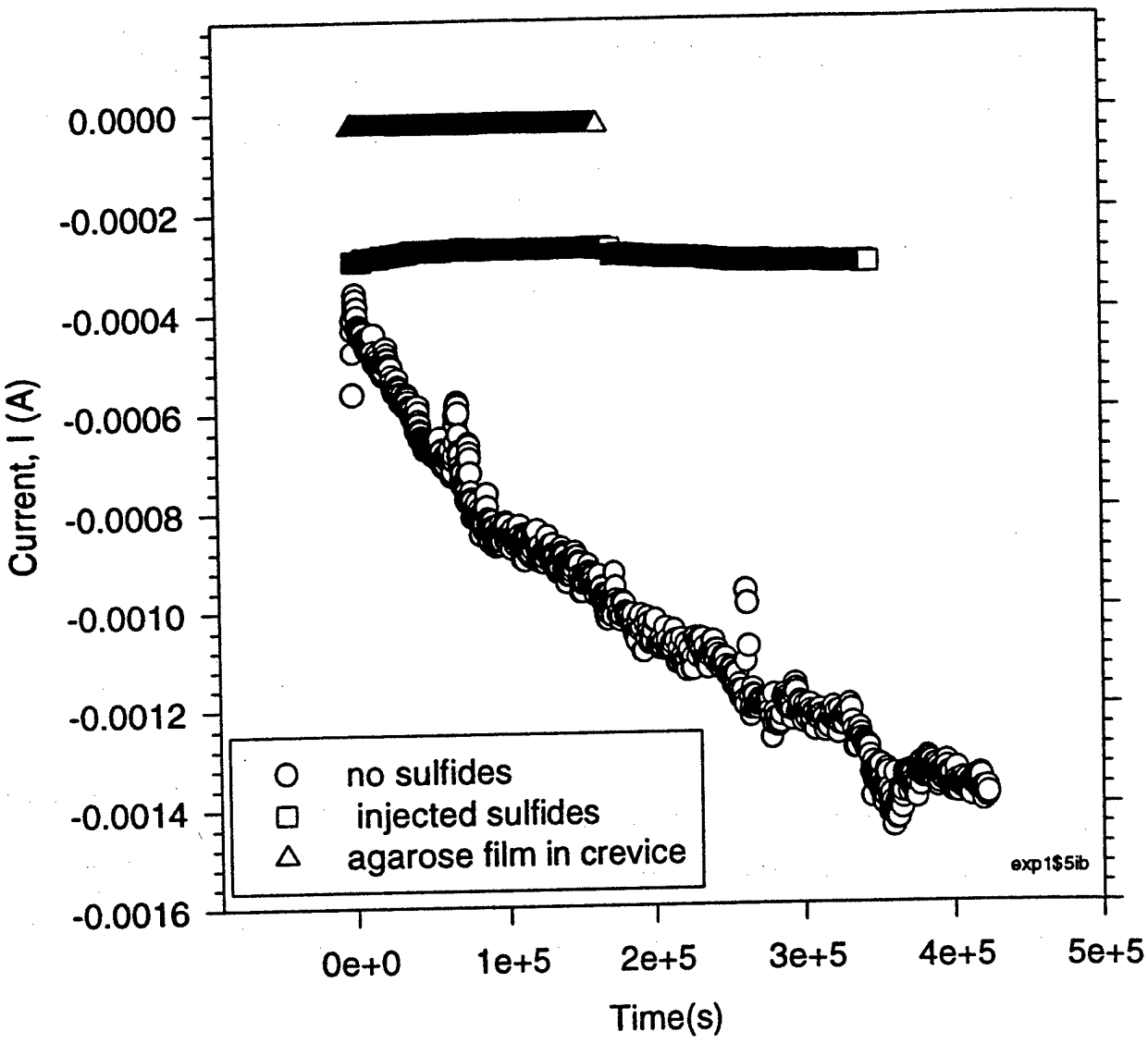

Figure 13: Current (A) vs. Time (s) during cathodic protection for crevice corrosion in 3.5 wt.% seawater, seawater with injected sulfides, and seawater with an agarose film inside the crevice.

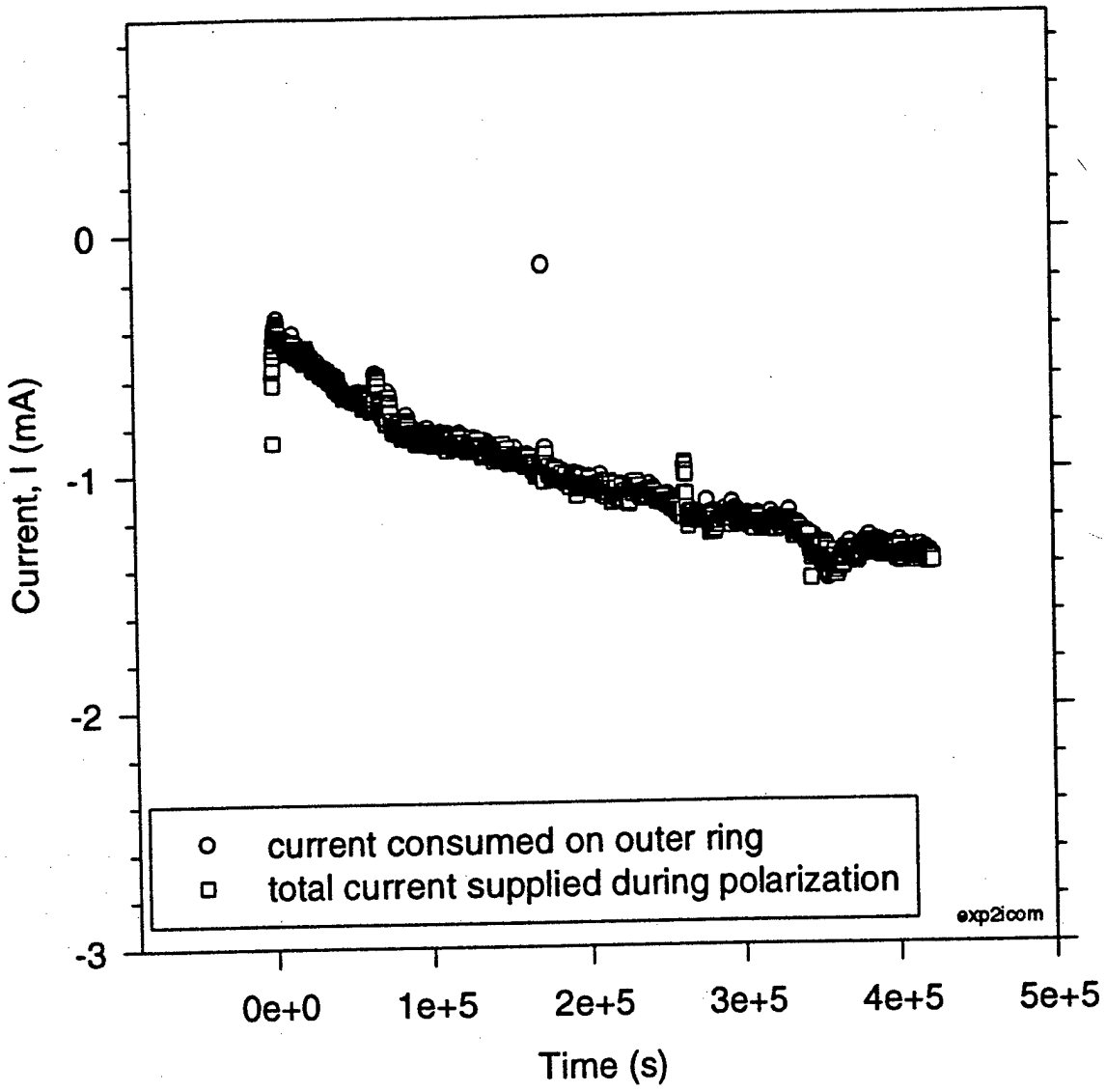

Figure 14: Current (mA) vs. Time (s) during cathodic protection in 3.5 wt.% seawater.

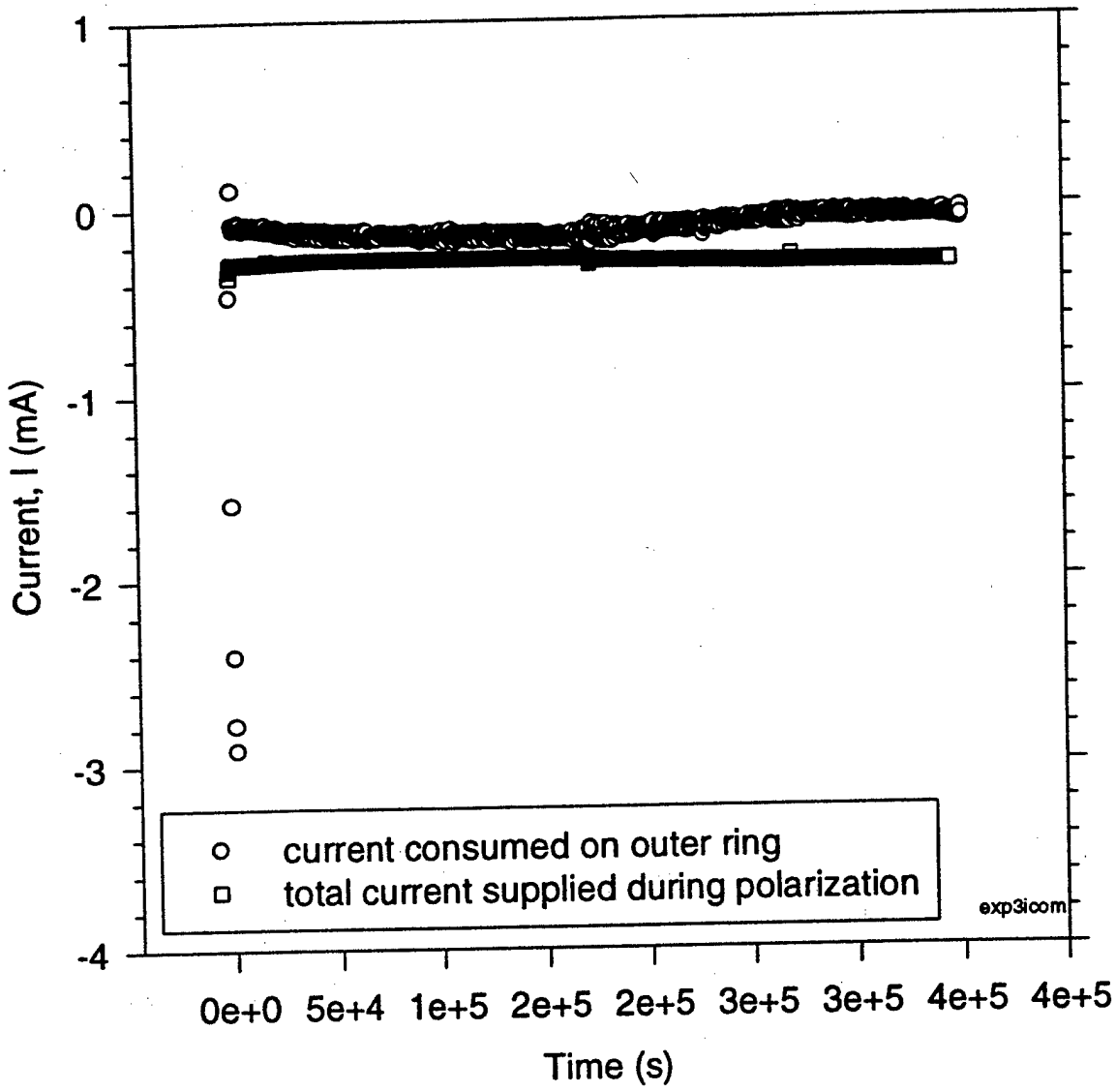

Figure 15: Current (mA) vs. Time (s) during cathodic protection in 3.5 wt.% seawater with injected sulfides.

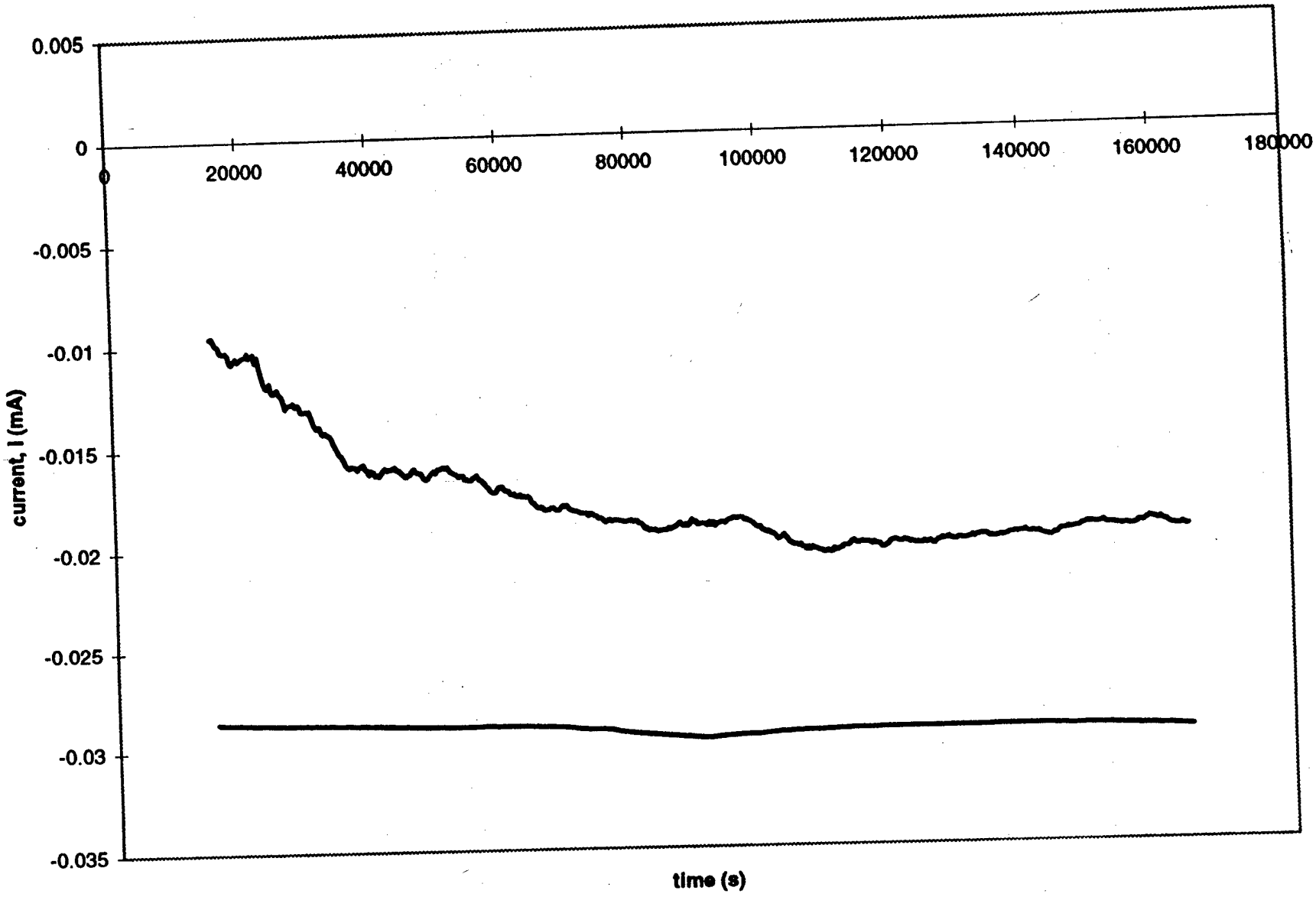

Figure 16: Current (mA) vs. Time(s) during cathodic protection in 3.5 wt.% seawater with an agarose film.

the crevice was relatively constant with time with negligible differences in measured potential between data points. See Figures 7, 8, and 9. The pH for each of the data points showed an increase over time from slightly acidic/slightly above neutral values into the range of relative alkalinity. pH values for the sulfide experiments, however, decreased but still remained quite alkaline. pH increased going into the crevice for the experiments with and without sulfides, but pH decreased going into the crevice for the experiments involving agarose. See Figures 17-19.

Discussion

The increasingly cathodic current from the potentiostatically protected steel sample seen in Figure 13 is evidence of the effectiveness of applied voltage cathodic protection in protecting against crevice corrosion in marine conditions. The increased cathodic current may be attributed to a further reduction of oxygen concentration inside the crevice so that the cathodic reaction occurring is only hydrogen evolution without oxygen reduction. It may also be attributed to the breakdown of the hydroxide film, exposing the bare underlying steel to the corrosive conditions. The majority of protective current supplied was consumed before it ever reached the crevice, as seen in Figures 14-16, due to possible counter electrode proximity and increased resistance of the crevice environment.

The potential ranges in Figures 7, 8, and 9 clearly demonstrate that the sample is thermodynamically protected from corrosion. The pH increases of Figures 17, 18, and 19 are clearly representative of a high rate of hydrogen evolution, possibly by the occurrence of the reaction:

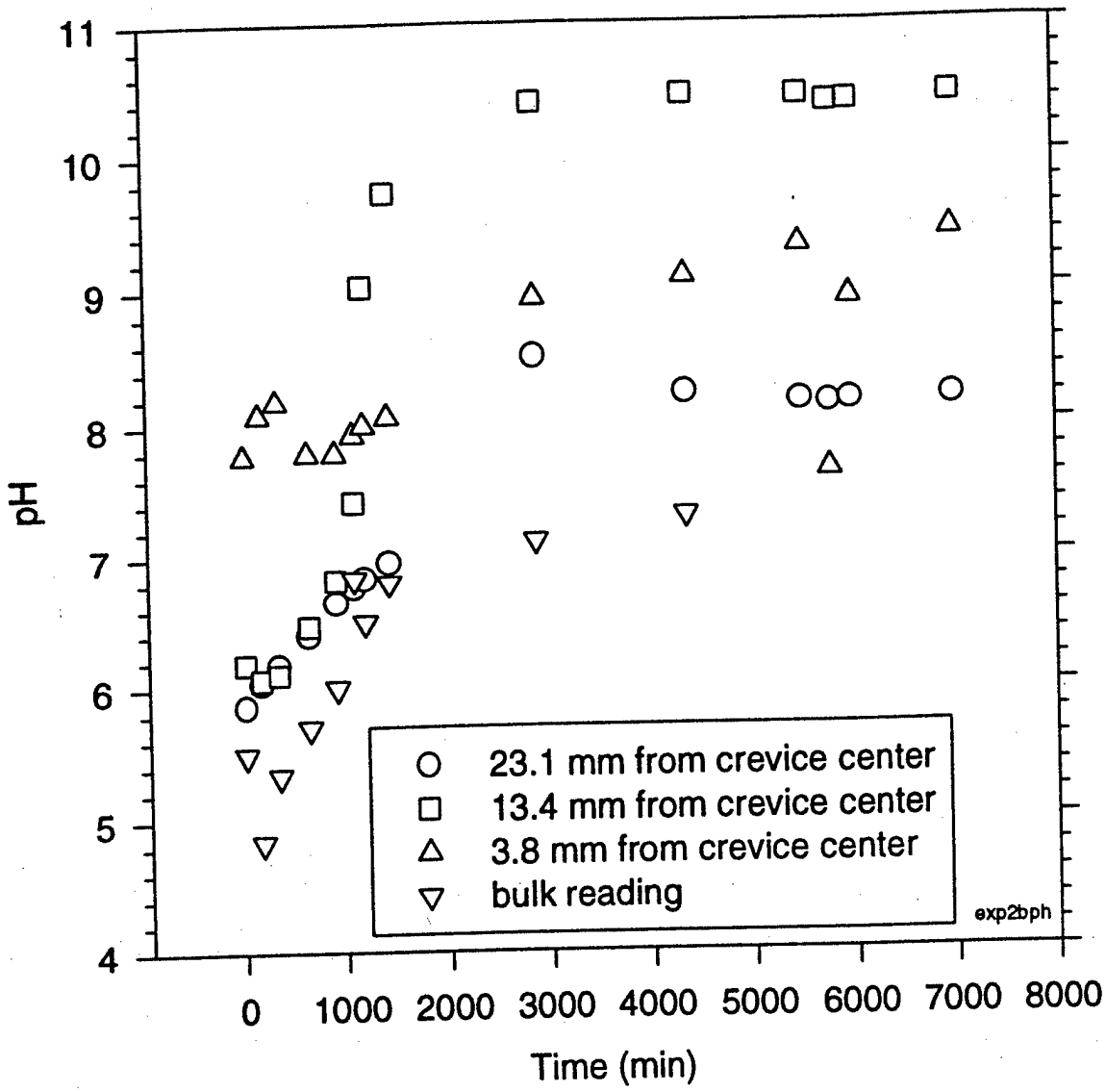

Figure 17: pH vs. Time (min) during cathodic protection in 3.5 wt.% seawater.

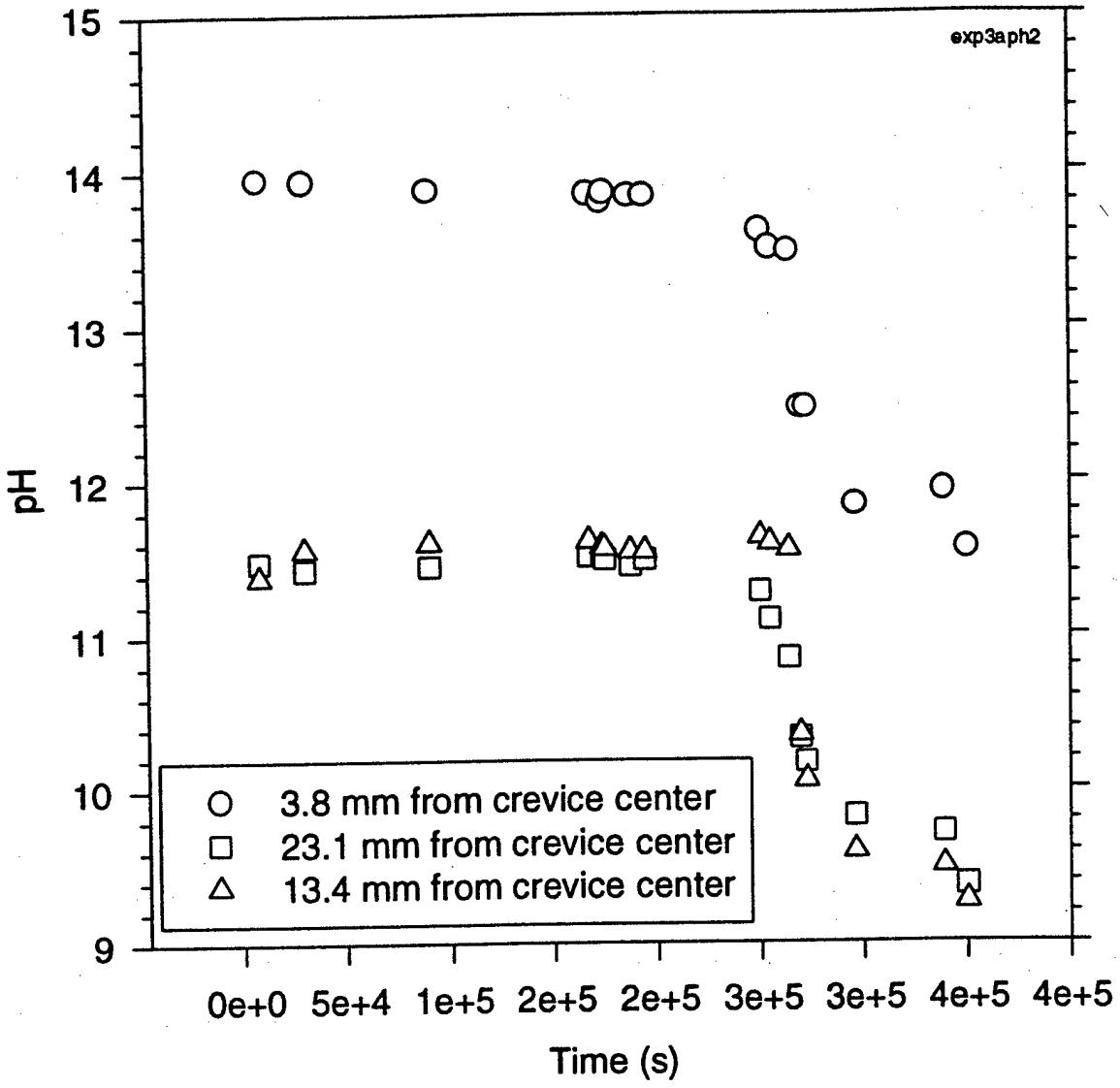

Figure 18: pH vs. Time (s) during cathodic protection in 3.5 wt.% seawater with injected sulfides.

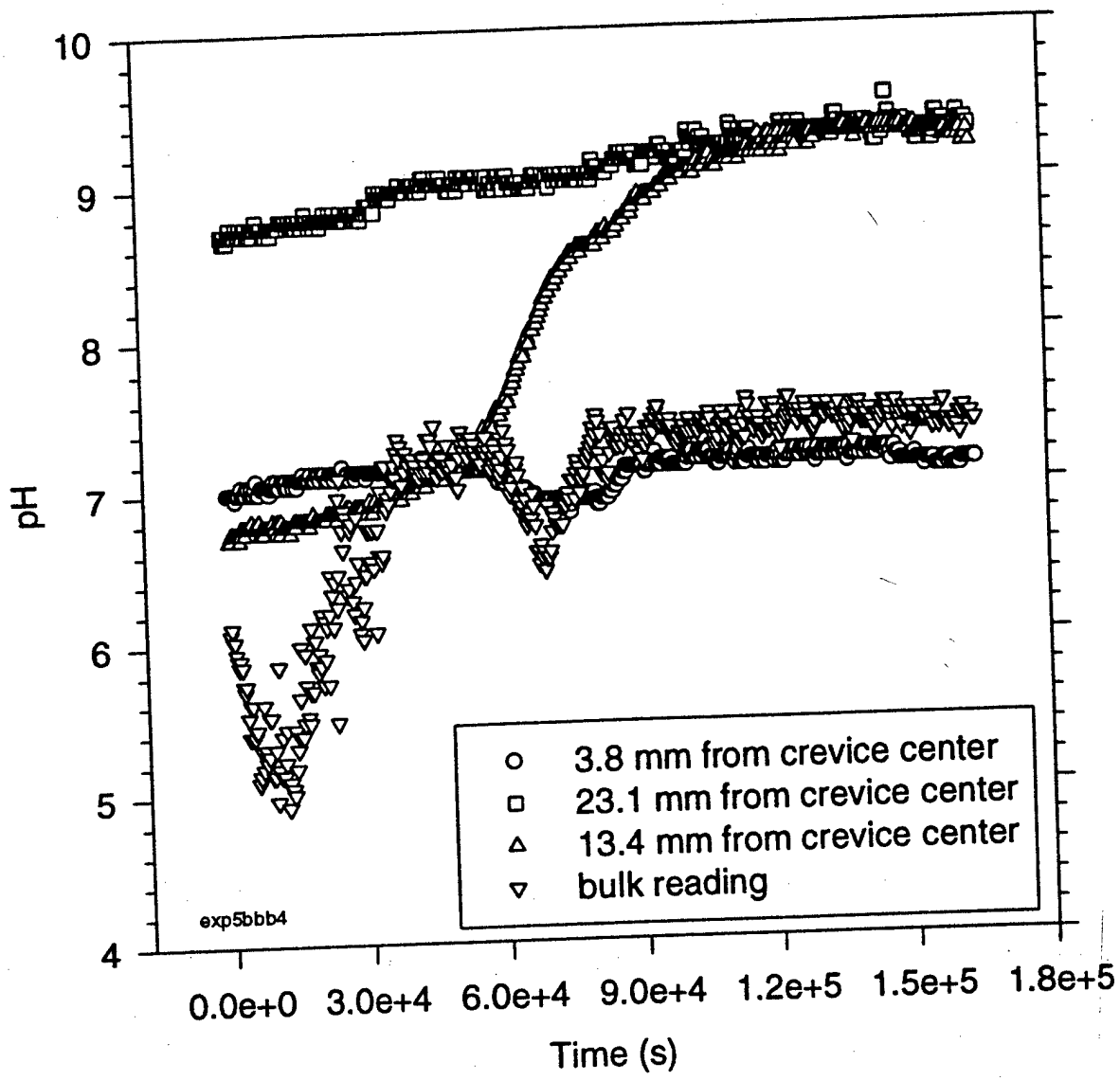

Figure 19: pH vs. Time (s) during cathodic protection in 3.5 wt.% seawater with an agarose film.

$$H_2O + e^- \rightarrow 1/2\ H_2 + OH^- \qquad (20)$$

which raises pH levels. pH decreased over time for the sulfide experiments due to the reaction $HS^- \rightarrow H^+ + S^{2-}$.

Figures 17-19 show the favorable effects of cathodic protection in that pH gradually changed from decreasing into the crevice to slightly increasing into the crevice, since H^+ ions would be consumed as soon as they enter the crevice. pH decreased going into the crevice for the agarose experiments possibly due to the increased resistance within the crevice.

ELECTROCHEMICAL IMPEDANCE SPECTROSCOPY (EIS)

Electrochemical Impedance Spectroscopy (EIS) experiments were run on the electrochemical cell in the presence of sulfides as well as in the presence of an agarose film. In EIS, a small excitation amplitude, sinusoidal voltage is applied to the working electrode in addition to the applied potential of interest. The response to this perturbation is called the impedance, which is the ac equivalent of dc resistance and is a function of the frequency of the perturbation. EIS data can reveal information on the kinetics at the interface, which in our case is the creviced metal/electrolyte interface or the creviced metal/simulated biofilm interface for the system containing sulfides or the agarose film, respectively. In the electrochemical cell, slow electrode kinetics, slow reaction rates for the chemical reactions, and diffusion can all impede electron flow, and can be considered analogous to the resistors, capacitors, and inductors that impede the flow of electrons in an ac circuit[16].

There are two common methods to analyze impedance data. Namely, the imaginary component can be plotted against the real component of the impedance in what is known as a Nyquist plot. Alternatively, the phase and magnitude can be plotted, simultaneously, against frequency in what is known as a Bode plot. Both plots are useful, but should be used in conjunction with each other in a thorough analysis of impedance data.

Kramers-Kronig (K-K) Transforms are used to test the validity of impedance data taken from electrochemical systems to ensure that the system satisfies the constraints of Linear Systems Theory, namely, linearity, stability, and causality[17]. A system is linear if the response to a sum of individual inputs is equal to the sum of the individual responses. A system is causal if it does not generate noise independent of the applied signal for $t \geq 0$. A system is unstable if it does not relax to its original state upon removal of the perturbation. We can define the complex impedance as

$$Z(j\omega) = V(j\omega)/I(j\omega) = Z'(\omega)-jZ''(\omega) \tag{21}$$

where $V(j\omega)$ and $I(j\omega)$ are the complex sinusoidal voltage and current, respectively, and $Z'(\omega)$ and $Z''(\omega)$ are the frequency-dependent real and imaginary components of the impedance. If the system of interest is stable, linear, and causal, then the K-K transforms must hold. The transforms are shown in equations 22 through 24:

$$Z'(\omega) = Z'(0) + (2\omega/\pi)\int[(\omega/x)Z''(x)-Z''(\omega)] * (1/(x^2-\omega^2)dx \tag{22}$$

$$Z'(\omega) = Z'(\infty) + (2/\pi)\int(xZ''(x)-\omega Z''(\omega)dx)/(x^2-\omega^2) \tag{23}$$

$$Z''(\omega) = -(2\omega/\pi)\int(Z'(x)-Z'(\omega)dx)/(x^2-\omega^2) \tag{24}$$

The calculation of equations 22 through 24 requires that the integrals can be calculated over the frequency range, x, from 0 to ∞. Since impedance data is measured

over a finite frequency range, namely, x_1 to x_2, it is necessary to insure that the integrals from 0 to x_1 and x_2 to ∞ are small compared to the integral from x_1 to x_2. if this is not the case, a "tails problem" is encountered and the data may lead to erroneous conclusions.

There are two methods by which the error due to the "tails problem" can be minimized. The first method requires extrapolating the impedance data to a frequency range greater than the one over which the data was acquired. These extrapolations are performed via polynomial fits to frequency values approximately 2 to 3 orders of magnitude above and below the measured frequency range. The second method involves limiting the K-K impedance to a smaller frequency range than the one used in data collection. Typically, this range has minimum and maximums approximately 2 to 3 orders of magnitude above and below, respectively, the measured frequency range.

The first method of reducing the error caused by the "tails problem" is effective when the polynomial used during extrapolation fits the measured data well even at low frequencies. When noise is a problem, however, that is, when low frequency points do not fit the polynomial well, the second method of limiting the K-K impedance data is the preferred method.

Results

The frequency range was originally set at 5000 Hz and decreased to 1 mHz with data points measured ten points every decade. The amplitude of the perturbation signal was 5 mV peak to peak above and below the cathodic protection potential. Phase and magnitude vs. frequency for the experiments with injected sulfides are plotted in Figures

20 and 21, respectively. Bode plots can provide information on the polarization resistance, R_p, and ohmic resistance, R_Ω, provided the magnitude plateaus at high and low frequencies. R_p is the polarization resistance or charge-transfer resistance at the electrode/solution interface. R_Ω is the ohmic or uncompensated resistance of the solution between the working and reference electrodes. The point at which the curve intersects the y-axis at the high frequency end of the plot corresponds to the value for R_Ω and the point at which the curve intersects the y-axis at the low frequency end is the sum of the values for R_p and R_Ω. It can be seen from Figure 21 that there is no plateau at either the high frequency or low frequency ends of the curve. Thus, it is difficult to ascertain what values R_Ω or R_p possess.

A Nyquist plot can provide information similar to that which is provided by the Bode diagram, although frequency data is not provided for in the Nyquist plot. The conventional shape of this plot on a planar electrode is a semicircle, with R_Ω measured at the left side of the semicircle where the imaginary component of the impedance is zero, which the high frequency end of the data range. The sum of R_p and R_Ω is measured at the opposite end of the semicircle where the imaginary component of the impedance is zero, which is the low frequency region of the data range. The semicircle often must be extrapolated in order to intersect the x-axis in this case, due to increased data scatter at lower frequencies as a result of system changes during the longer data acquisition times. The Nyquist plot in Figure 22 does not form a semicircle, as the low frequency end of the data spectra continues to increase with decreasing frequency. The value for R_Ω appears to be approximately 14.0 Ω.

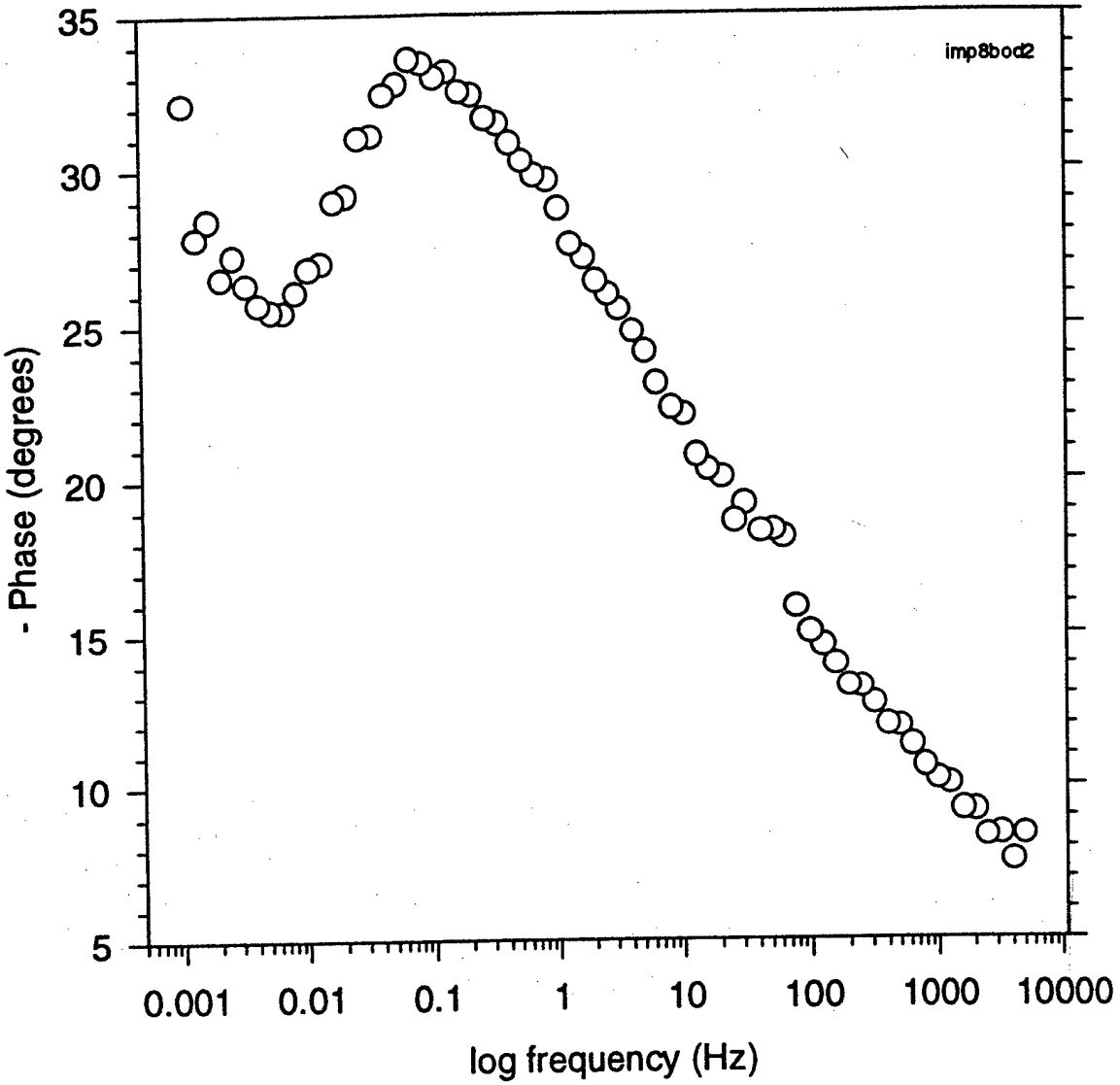

Figure 20: Phase (degrees) vs. Frequency (Hz) in a Bode plot for 3.5 wt% seawater with injected sulfides.

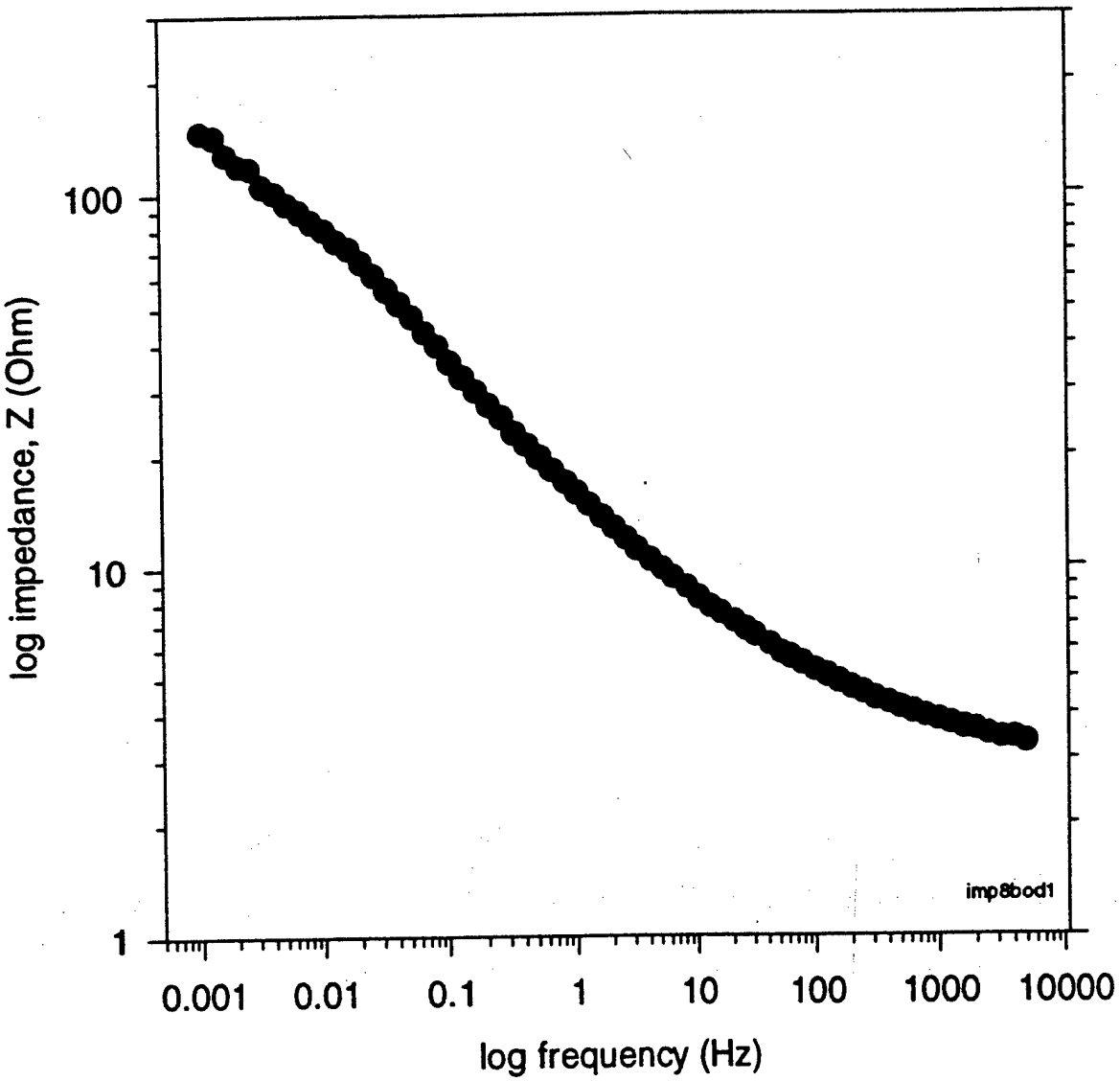

Figure 21: Impedance magnitude (Ohm) vs. Frequency (Hz) in a Bode plot for 3.5 wt% seawater with injected sulfides.

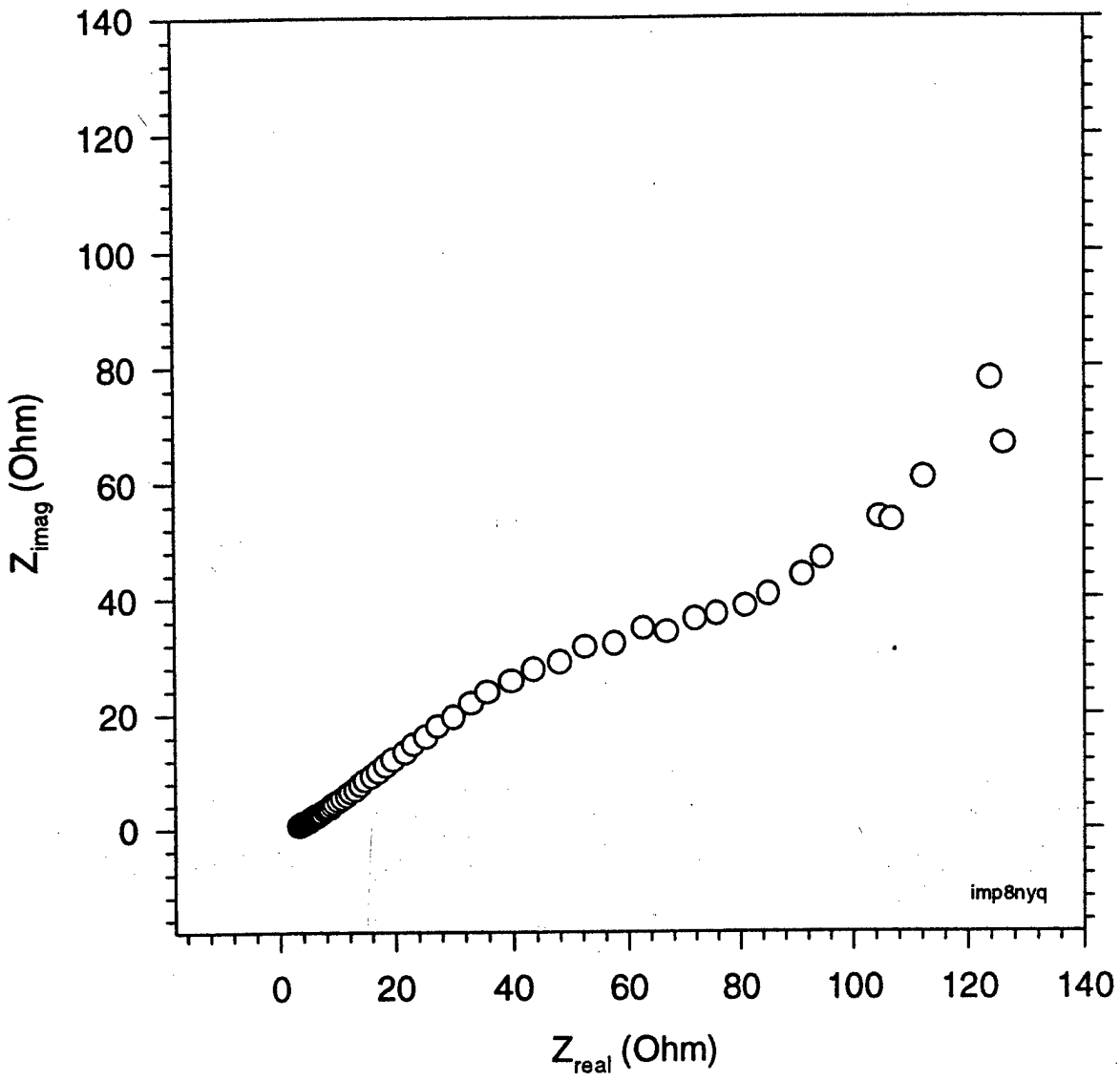

Figure 22: Real vs. Imaginary components of impedance (Ohm) in a Nyquist plot for 3.5 wt% seawater with injected sulfides.

The Kramers Kronig Transforms for the real and imaginary components of the impedance data are shown in Figures 23 and 24, respectively. Again, the greatest scatter in the data is at lower frequencies. The correlation coefficients for Figure 23 is 0.99727 while that for Figure 24 is 0.91555. Extrapolation of the real and imaginary components of the impedance data to account for the "tails" yields correlation coefficients of 0.98178 and 0.73751, respectively. Limiting the data field to a smaller frequency range, as per the second method of handling the "tails problem", yields correlation coefficients of 0.99094 and 0.82195 for the real and imaginary components of the impedance, respectively.

The Bode, Nyquist and K-K Transform plots for the experiments run with an agarose film are shown in Figures 25, 26, 27, 28, and 29. The value for R_Ω from the Nyquist plot was approximately 1400.0 Ω, but was indeterminable from the Bode plot. The value for R_p was indeterminable from either the Nyquist or Bode diagrams. The K-K transform correlation coefficients for the real and imaginary components of impedance were 0.98538 and -0.72819, respectively. Since there was significant noise at the low frequency end of the impedance data, the extrapolation method was not a viable option in handling the "tails problem". Therefore, the data field was limited to a frequency range within the measured frequency range, yielding correlation coefficients of 0.80204 and 0.60886 for the real and imaginary components of the impedance, respectively.

Discussion

The magnitude of the impedance changed by several orders of magnitude when the system was changed from sulfide injection to the agarose film. This is an indication of the increased resistance to electrolyte flow, due to the presence of a biofilm or tubercle on the

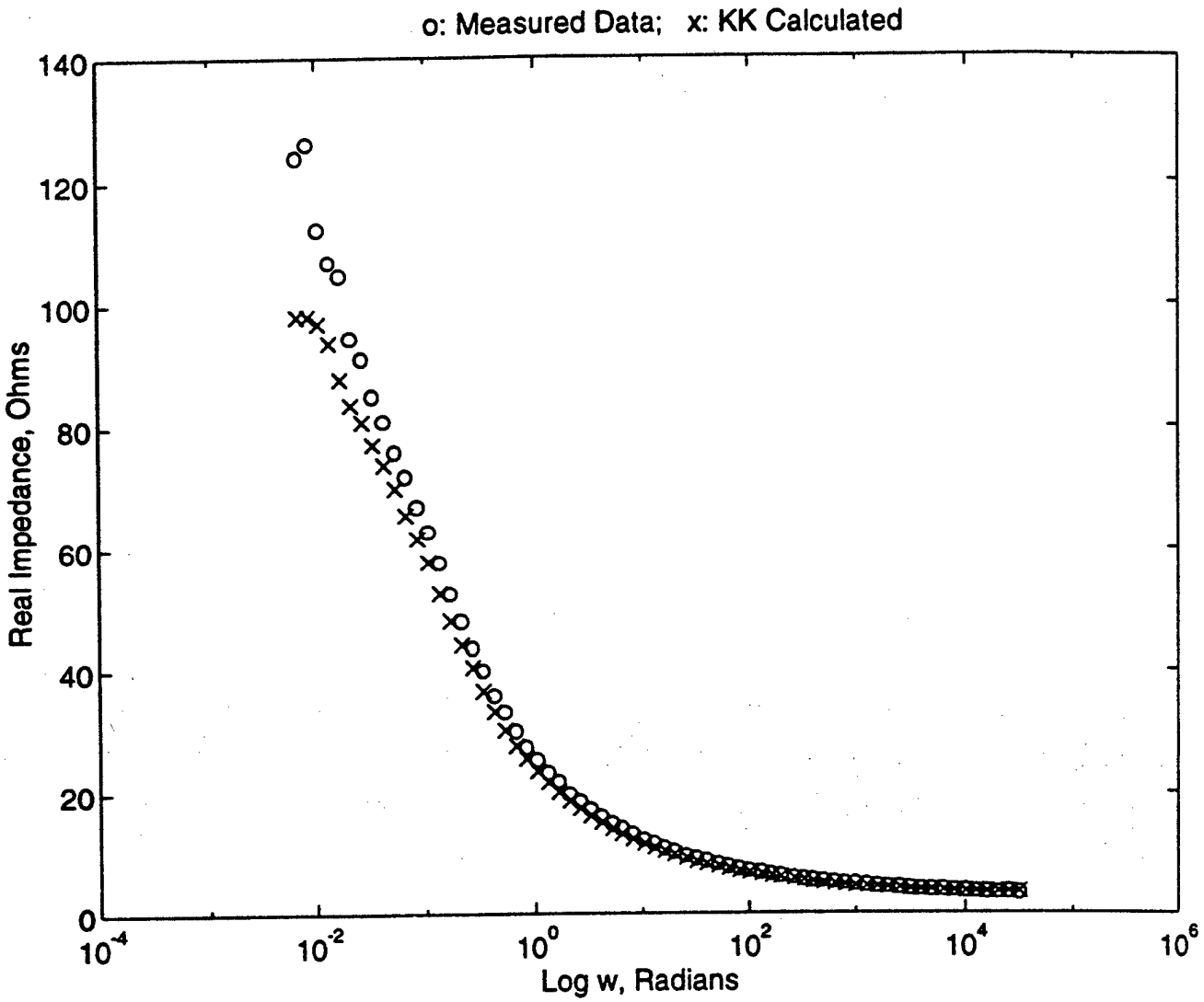

Figure 23: Imaginary to Real K-K Transform for experiments in 3.5 wt.% seawater with injected sulfides.

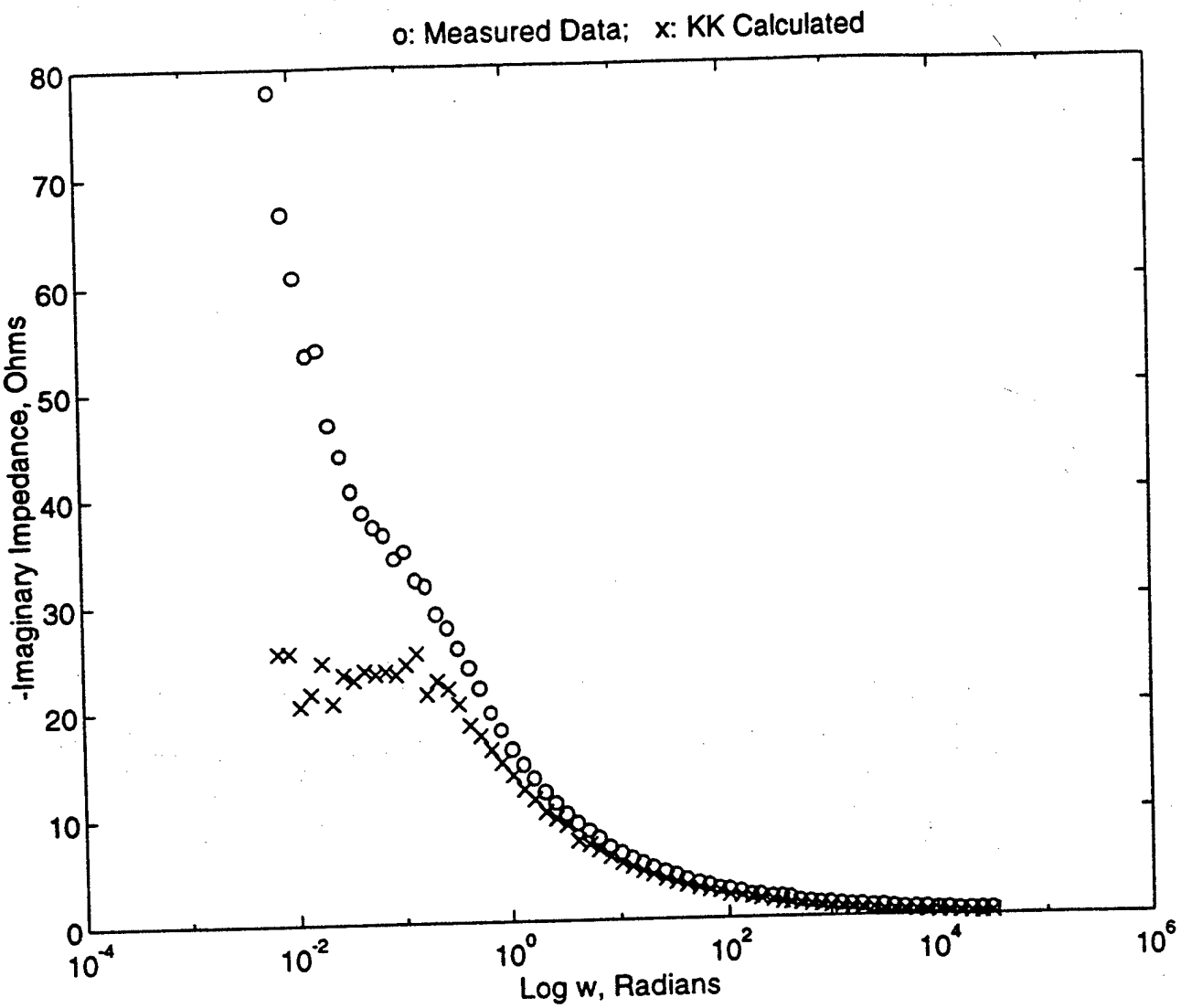

Figure 24: Real to Imaginary K-K Transform for experiments in 3.5 wt.% seawater with injected sulfides.

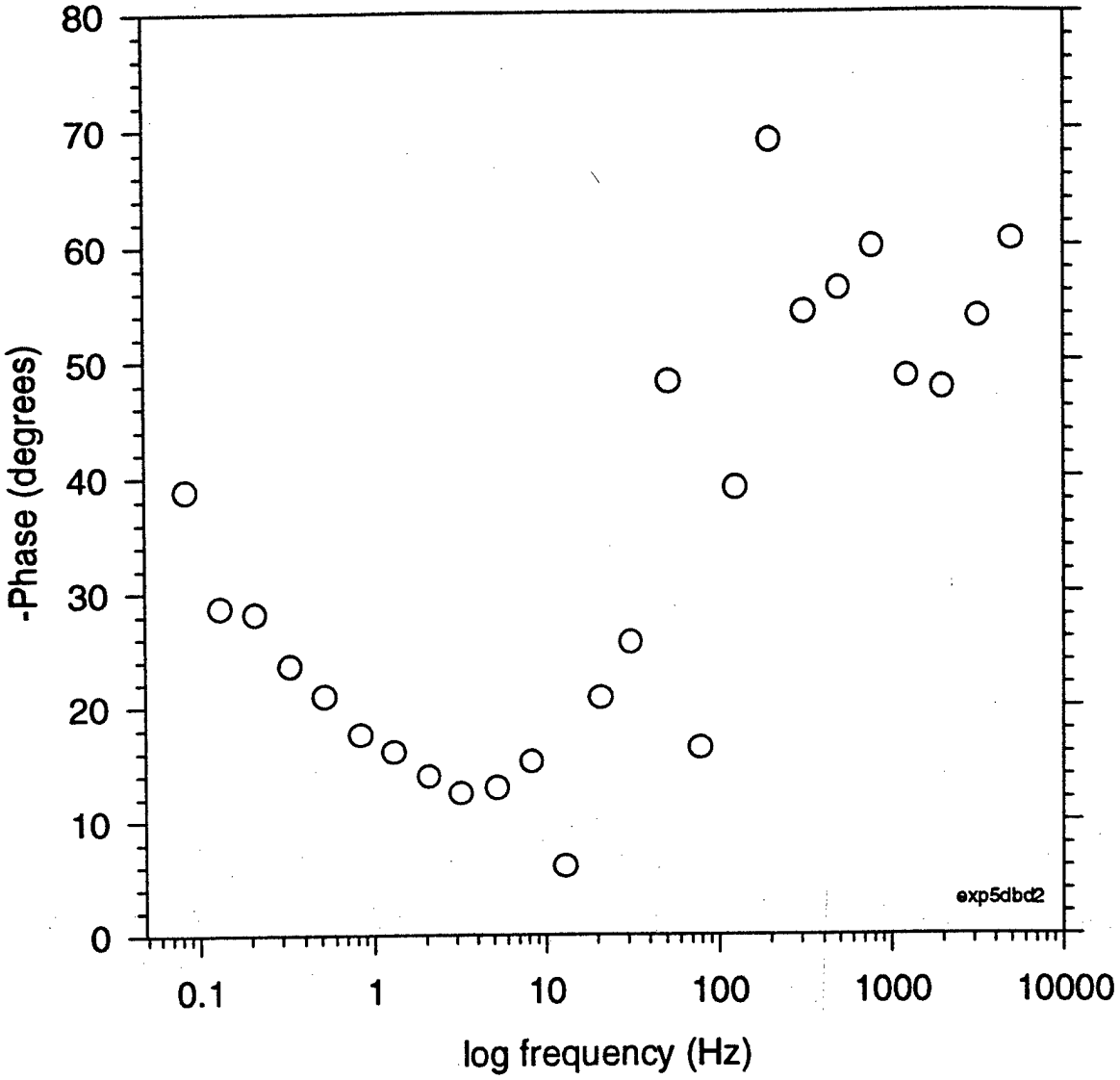

Figure 25: Phase (degrees) vs. Frequency (Hz) in a Bode plot for 3.5 wt% seawater with an agarose film.

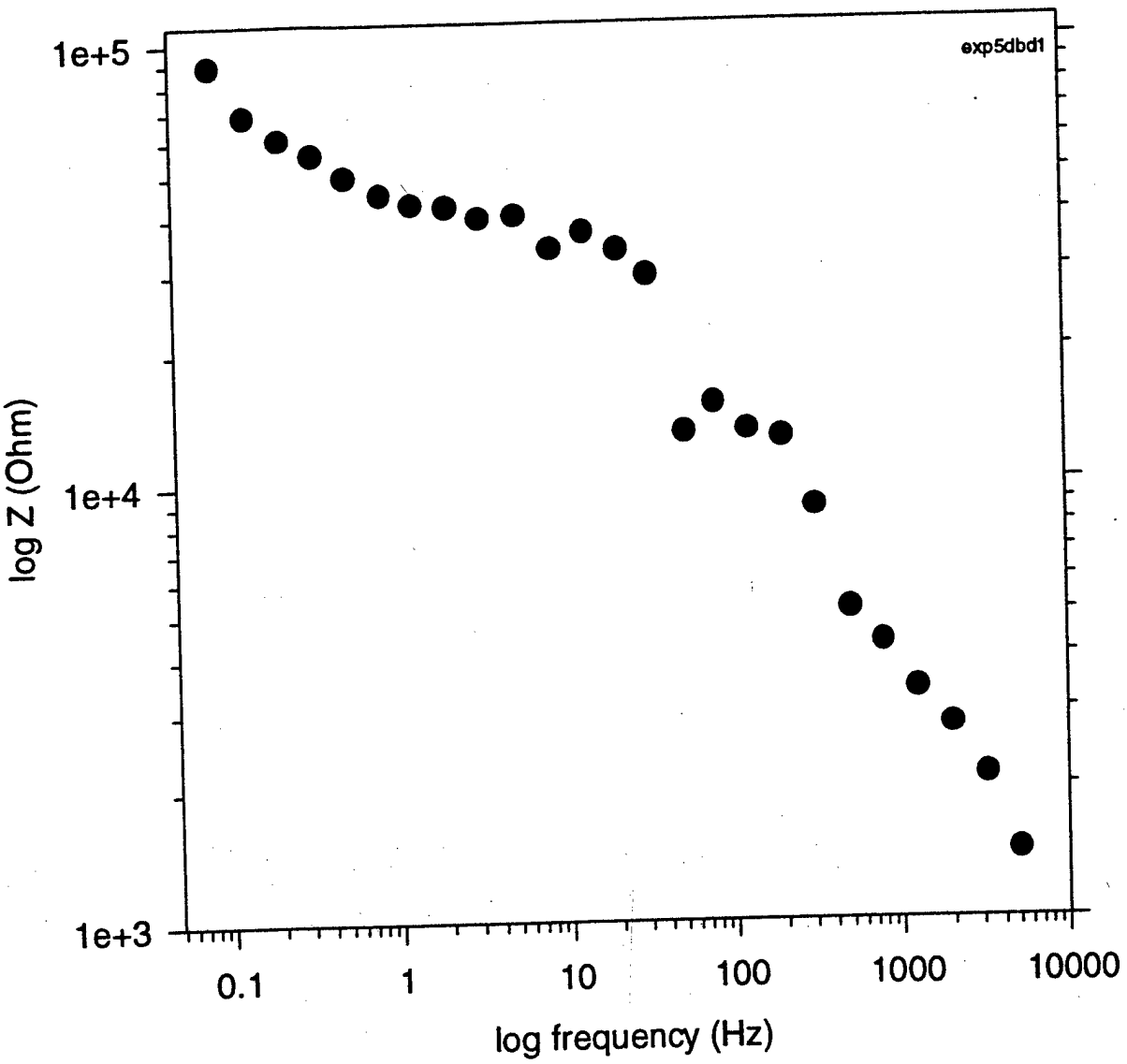

Figure 26: Impedance magnitude (Ohm) vs. Frequency (Hz) in a Bode plot for 3.5 wt% seawater with an agarose film.

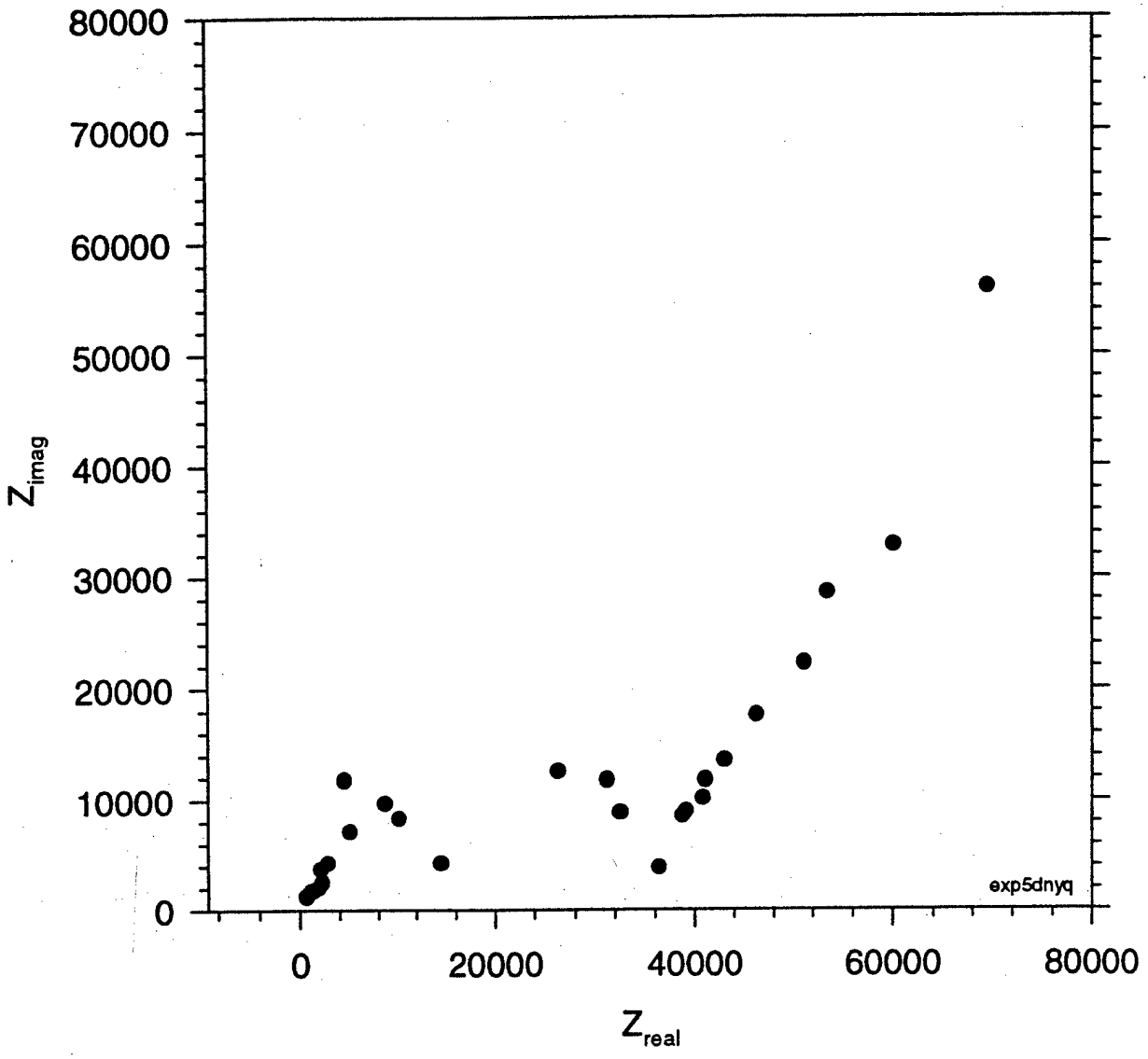

Figure 27: Real vs. Imaginary components of Impedance (Ohm) in a Nyquist plot for 3.5 wt% seawater with an agarose film.

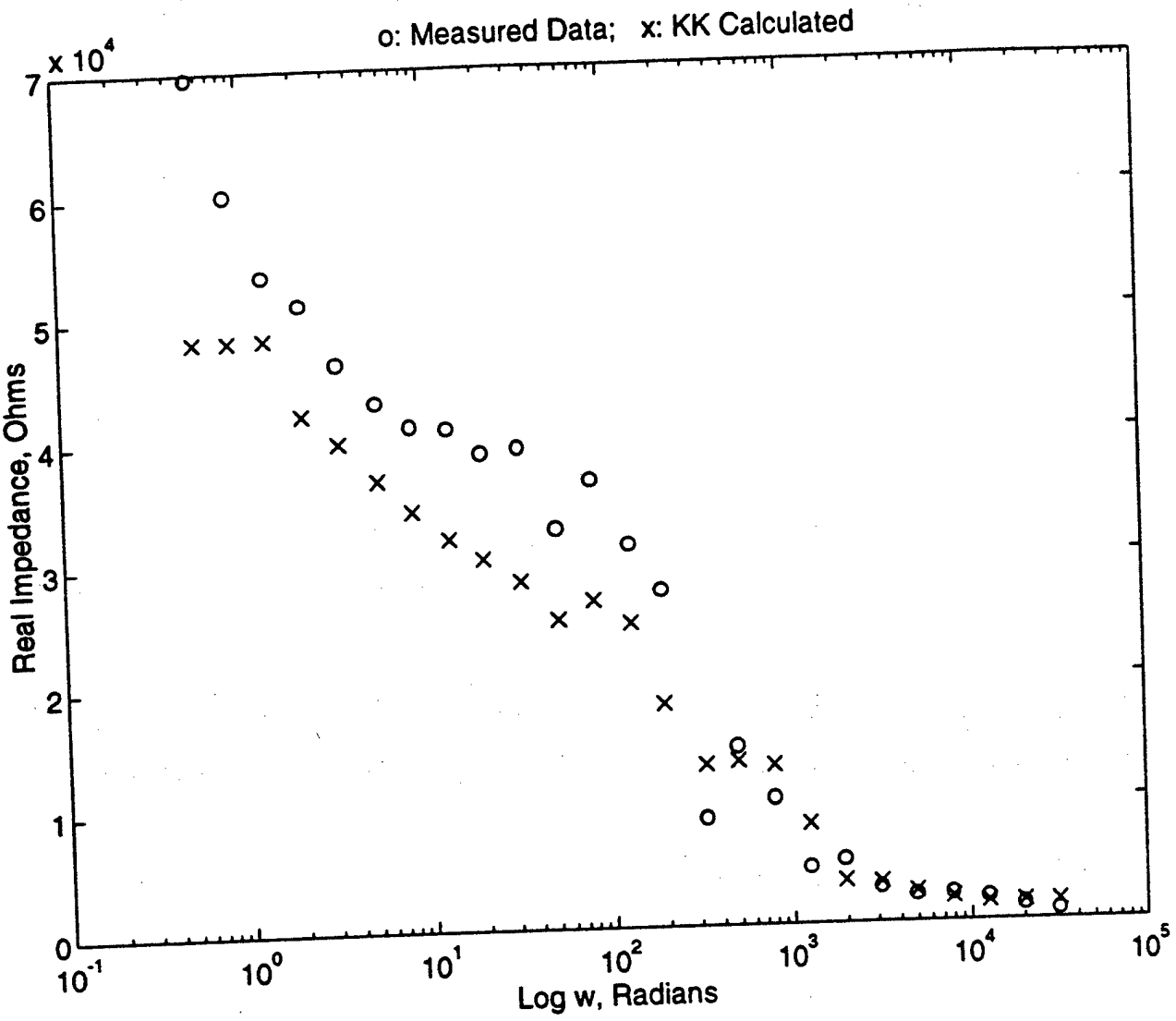

Figure 28: Imaginary to Real K-K Transform for experiments in 3.5 wt.% seawater with an agarose film.

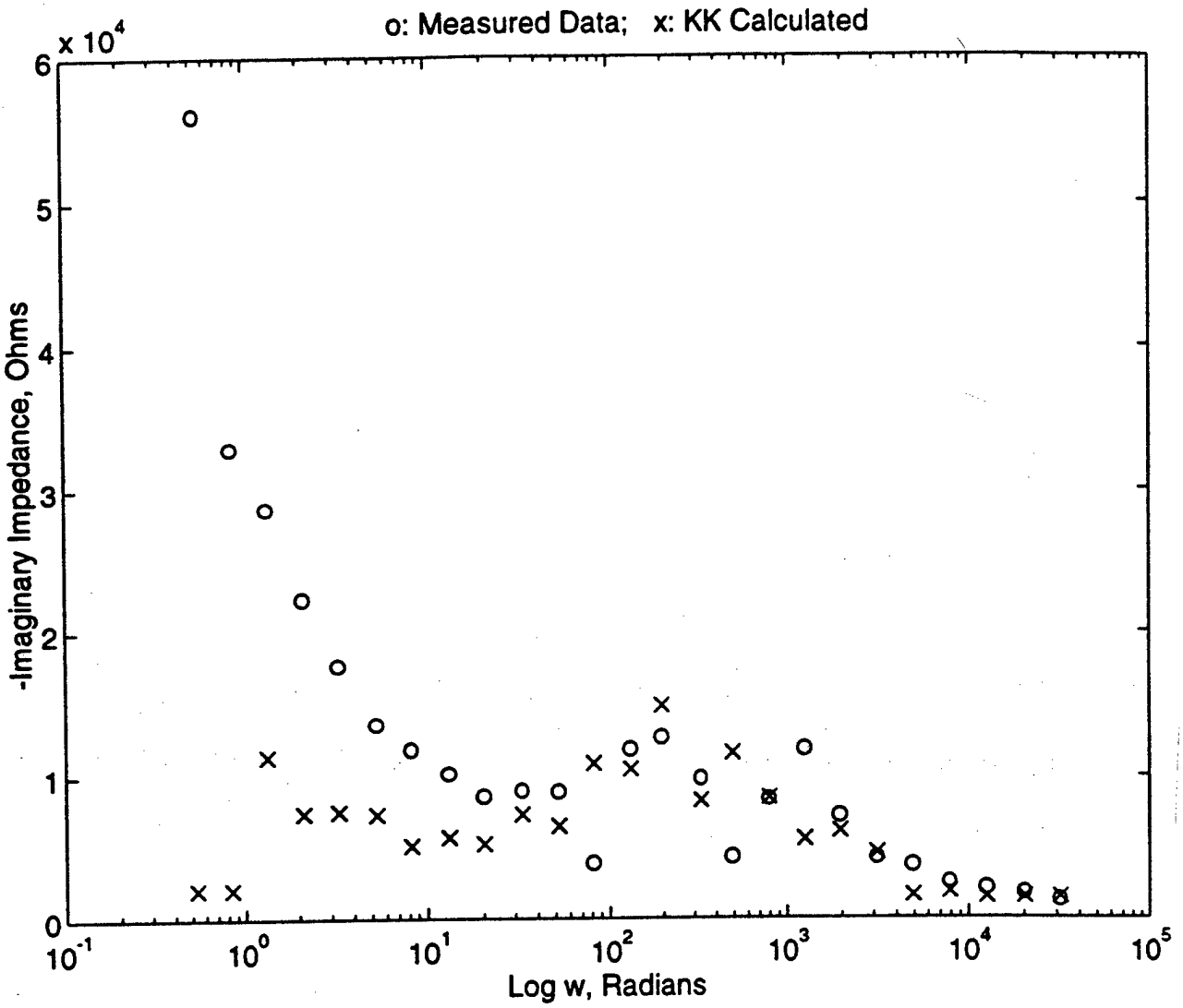

Figure 29: Real to Imaginary K-K Transform for experiments in 3.5 wt.% seawater with an agarose film.

steel surface. Such a resistance can also trap corrosion products at the metal surface, causing severe conditions leading to enhanced corrosion. The use of the Stern-Geary Equation:

$$i_{corr} = [\beta_a \beta_c / 2.303(\beta_a + \beta_c)](1/R_p) \quad (25)$$

allows a direct relationship between the steady state corrosion current density and the polarization resistance, R_p. The value for R_p appears to be much greater for the experiments run with the agarose film. It can, therefore, be reasoned that the corrosion rate was greater with the injected sulfides rather than with the agarose film. This correlates to the current data measured during cathodic protection where the amount of necessary protective current was greater in the case of the injected sulfides relative to the agarose film.

The true value for R_p is buried in the impedance data. This is due to the nature of the system under consideration. That is, the corrosion products that build up during open circuit experiments can be evaluated in terms of porous films. These films exhibit a strong influence on the EIS behavior of the corroding surface[18]. For porous systems, the phase angle varies from 45° at infinite frequency to 0° at zero frequency, whereas the conventional plane electrode displays phase angle ranging from 90° at infinite frequency to 0° at zero frequency. In addition, if Z is a diffusional impedance the phase angle becomes 22.5° assuming an infinitely long pore. The Nyquist plots in Figures 22 and 27 display such behavior described above. The deviation of the impedance data from expected values in the case of the agarose film experiments may also be due to the presence of more than one time constant.

MODEL

A transmission line electrical analog for the crevice has been developed, which will be utilized to interpret electrochemical impedance data generated from a Gamry™ CMS300 Impedance software system. From Figure 30, it can be seen that the penetration length of the applied signal depends on the frequency of the perturbation. Using the equation $Z = (1/j\omega c)$, where Z is the impedance and ω is the angular frequency, it can be seen that by raising or lowering the frequency, the impedance across the metal/solution interface will be lowered or raised, respectively. The same argument holds for a more complicated electrical analog for the steel/solution interface. For our model, the resistance, R, is dependent on the concentration of ions in the electrolyte, and the impedance, Z, is dependent on the corrosion rate. When impedance is low and the resistance, R, is high, the current, I, drops off a short distance into the crevice. When impedance is high and the resistance, R is low, the current, I, can be injected further into the crevice. In this way, it is possible to interrogate the crevice to different depths, and hence to determine the effectiveness of impressed current cathodic protection against crevice corrosion and MIC.

The transmission line model[19] for the test cell employs radial symmetry, which is the simplest geometrical description of a tubercle on a macro scale. The radius of the crevice will be denoted r_c. The radius of the opening into which sulfide solution flows is denoted r_0. It is assumed that the potential of the metal phase is constant, while the potential in the solution phase, V(r), is dependent on the distance, r, within the crevice. Applying both Ohm's (E = IR) and Kirchoff's ($I_{in} = I_{out}$) laws to any circular ring above

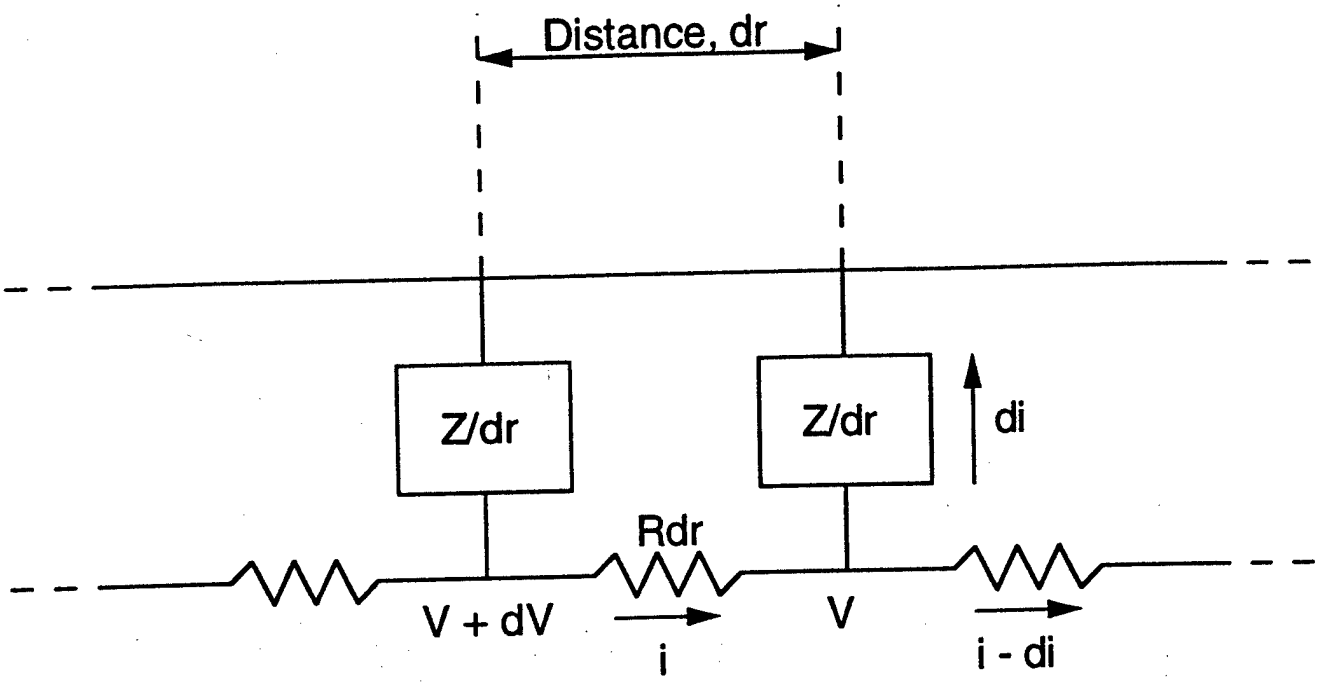

Figure 30: Small increment dr of the transmission line for the crevice, where R is the solution resistance per unit length and Z is the crevice wall/solution impedance per unit length.

the disk-shaped crevice, seen in Figure 31, of internal radius r and external radius r+dr, equations for the potential V(r) and the current i(r) are obtained as follows:

$$V-(V+dV) = R_S i(r), \text{ where } R_S = \rho dr/2\pi rh$$

$$\text{rearranging, } dV(r)/dr = -\rho i(r)/2\pi rh \tag{26}$$

$$\text{Similarly, } 0-V = Z_e di/dr, \text{ where } Z_e = Z_l/2\pi r$$

$$\text{rearranging, } di(r)/dr = -2\pi r V(r)/Z_l \tag{27}$$

In the above equations, R_S is the resistance of an element dr above the crevice, ρ is the solution resistivity, Z_e is the impedance in units of ohm*cm, and Z_l is the normal impedance of the metal/solution interphase in units of ohm*cm^2. By differentiating equation (16),

$$d^2V(r)/dr^2 = -(\rho/2\pi h)[(rdi(r)-i(r))r^2]$$

$$= -(\rho/2\pi h)[(-2\pi r^2 V(r)/Z_l + 2\pi rhdV(r)/\rho dr)/r^2]$$

$$= -dV(r)/rdr + \rho V(r)/hZ_l \tag{28}$$

By differentiating equation (17),

$$d^2i(r)/dr^2 = -(2\pi/Z_l)[rdV(r)/dr + V(r)]$$

$$= -(2\pi/Z_l)[-r\rho i(r)/2\pi rh - Z_l di(r)/2\pi rdr]$$

$$= di(r)/rdr + \rho i(r)/Z_l h \tag{29}$$

By making the transformation $x = r\rho/Z_l h$, these equations can now be written as

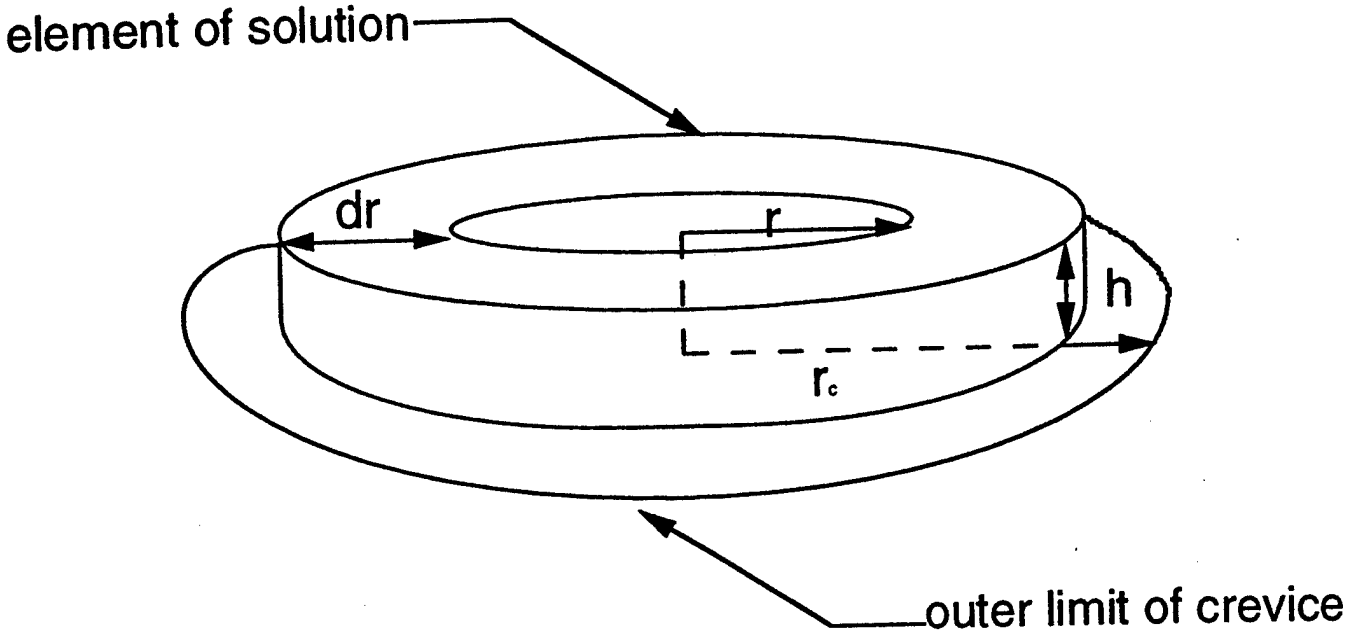

Figure 31: Arbitrary circular element of solution within the crevice, where h is the height of the crevice, r is the inner diameter of the element of solution, r+dr is the outer diameter of the element of solution, and rc is the radius of the crevice.

$$f''(x) = -f'(x)/x + f(x) \tag{30}$$

where f is either V or i. This corresponds to the modified Bessel Equation with solutions given by

$$f(x) = AI_0(x) + BK_0(x) \tag{31}$$

where $I_0(x)$ and $K_0(x)$ are the modified Bessel functions of zero-order. The integration constants A and B are given by the boundary conditions for V and i:

$$I(x_c) = I_{applied} \qquad I(x_0) = 0 \tag{32}$$

$$(dV(x)/dx)_{x=xo} = 0 \quad (dV(x)/dx)_{x=xc} = -I(x_c)\rho/2\pi x_c h \tag{33}$$

where x_c is the value of x corresponding to r_c and x_0 is the value of x corresponding to r_0. The total impedance of the metal surface can now be given by:

$$Z_T = (V(x_c)/I(x_c))_{x=xc} \tag{34}$$

The values of $V(x_c)$ and $I(x_c)$ are provided for in the Appendix, as calculated by the Mathematica™ software language, as is the calculated value of Z_T. For our model, r_c = 2.54 cm, r_0 = 0.11938 cm, h = 0.02 cm, and $\rho = 3.095975*10^6\Omega$.

By determining a value for Z_T, it is possible to compare experimental data to calculated data and compare, modifying the mathematical model accordingly. In this way, it will be possible to develop an optimization technique through our model, and thus

predict the current or potential necessary to cathodically protect the creviced steel sample from corrosion.

FUTURE WORK

Open circuit and cathodic polarization experiments revealed the effectiveness of cathodic protection in eliminating crevice corrosion in marine environments. One major drawback of cathodic protection is the increased production of hydrogen, which may be absorbed into the steel substrate, thus producing the danger of hydrogen embrittlement. In environments containing SRB, an additional cause of hydrogen absorption into the substrate may be the metabolic activities of these bacteria. One common method of preventing the deleterious effects of SRB is to increase the degree of applied voltage, which has its own deleterious effect in promoting hydrogen absorption.

Indeed, Robinson and Kilgallon[20] observed that cathodic potentials used to protect steel from corrosion also promote entry of hydrogen into the substrate. Their experiments were run in near-neutral marine solutions, with SRB and without SRB. Pankhania[21] suggested that the increased concentration of hydrogen at the protected substrate leads to increased levels of microbial activity, leading to production of destructive sulfides, leading to increased corrosion. Thus, an important issue that must be addressed is to discover the potential at which corrosion (crevice, differential aeration, MIC) in marine environments is thermodynamically impossible without injection of substantial amounts of hydrogen into the substrate.

These experiments will be performed under anaerobic conditions in a glove box that has been reconstructed to allow leads in and out for polarization. Finally, live cultures of SRB will be incorporated into the cell and results will be compared to results obtained abiotically, in order to determine the deleterious effects of MIC, in *addition* to sulfide production.

In order to improve the experimental techniques, additional experiments are planned using microreference electrodes probing the underside of the creviced sample. In this manner, the crevice environment itself remains undisturbed and more accurate, in situ readings may be obtained.

REFERENCES

1. **Pope, D.H., D.J. Duquette, A.H. Johannes, and P.C. Wayner. 1984.** Materials Performance, Vol. 23, No. 4, p. 14.

2. **Kuhr, Wolzogen, C.A.H. Von, and L.S. Van der Vlugt. 1934.** Water, Den Haag, Vol. 18, p. 147.

3. **Little, B., P. Wagner, and F. Mansfeld. 1992.** Electrochimica Acta, Vol. 37, No. 12, p. 2185.

4. **Costerton, J.W., Cheng, K.J., Geesey, G., Ladd, T.I., Nickel, J.C., Dasgupta, M., T.J. Marrie. 1987.** Bacterial biofilms on Nature and Disease. Ann Rev. Microbiol. Vol. 41, p. 435-464.

5. **Flemming, H.-C. 1991.** Introduction: Biofilms as a particular form of microbial life. pp. 1-6, *In* H. Flemming and G.G. Geesey (eds.), Biofouling and Biocorrosion in Industrial Water Systems. Springer Verlag., New York, NY

6. **Marshal, K.C. and B.L. Blainey. 1991.** Role of bacterial adhesion in biofilm formation and biocorrosion. pp. 29-46, *In* H. Flemming and G.G. Geesey (eds.), Biofouling and Biocorrosion in Industrial Water Systems. Springer Verlag., New York, N.Y.

7. **Rosenberg, M. and S. Kjelleberg 1986.** Hydrophobic interactions: Role in bacterial adhesion. pp. 353-393, *In* K.C. Marshall (ed.), Advances in Microbial Ecology.

8. **Postgate, J.R. (ed.), 1984.** The Sulfate Reducing Bacteria. 2nd ed. Cambridge University Press, Cambridge.

9. **Ford, T. and R. Mitchell. 1990.** The ecology of microbial corrosion. pp. 231-262, *In* K.C. Marshall (ed.), Advances in Microbial Ecology.

10. **Smith, J.S., and J.D.A. Miller. 1975.** British Corrosion Journal, Vol. 10, No. 3, p. 136.

11. **Shreir, L. L. 1976.** Corrosion, Volume 1, Metal/Environment Reactions. Newnes-Butterworths Press, London, Chp. 1.6, p. 1:130.

12. **Leidheiser, Jr., H., R.D. Granata, G. Fey, and M. Ingle. 1988.** Corrosion Science, Vol. 28, No. 6, p. 631.

13. **Pourbaix, M. 1970.** Corrosion, Vol. 26, No. 10, p.431.

14. Pickering, H. W., and R.P. Frankenthal. 1972. Journal of the Electrochemical Society, Vol. 119, No. 10, p. 1297.

15. Peterson, M.H., and T.J. Lennox, Jr. 1973. Corrosion, Vol. 29, No. 10, p. 406.

16. EG&G Princeton Applied Research. "Basics of Electrochemical Impedance Spectroscopy (EIS)", Application Note AC-1.

17. Urquidi-Macdonald, M., S. Real, and D.D. Macdonald. 1990. Electrochimica Acta, Vol. 35, No. 10, pp. 1559-1566.

18. Macdonald, D.D. 1990. Corrosion, Vol.46, No. 3, pp.229-242.

19. Macdonald, D.D., M. Urquidi-Macdonald, C. Diaz, A.C. Ramamurthy, W.J. van Ooij, A. Sabata, M. Strom, and G. Strom. 1993. "Interpretation of Electrochemical Impedance Data for Damaged Automotive Paint Films", 12th International Corrosion Congress, Houston, TX.

20. Robinson, M.J., and P.J. Kilgallon. 1994. Corrosion, Vol. 50, No. 8, p. 626.

21. Pankhania, I.P., A.N. Moosavi, and W.A.J. Hamilton. 1986. General Microbiology, Vol. 132, p. 3357.

Appendix

Note: $Z = x_c = r_c\alpha^{1/2} = 2.54\alpha^{1/2}$ and $z = x_0 = r_0\alpha^{1/2} = 0.11938\alpha^{1/2}$

$$\int dV(x_c) = \frac{6.96594\ 10^{7}\ \text{Log}[x]}{\text{Pi}}$$

$V(x_c) =$

```
(-1. BesselJ[0, I x]
   (0.375043 z BesselY[0, 2.54 I Z] -
      6.96594 10^7 BesselY[0, 0.11938 I z]
       Log[2.54 Z])) /
  (3.14159 BesselJ[0, 2.54 I Z]
     BesselY[0, 0.11938 I z] -
    3.14159 BesselJ[0, 0.11938 I z]
     BesselY[0, 2.54 I Z]) +
 BesselY[0, I x] (0.11938 z / BesselY[0, 0.11938 I z] +
   (BesselJ[0, 0.11938 I z]
      (0.375043 z BesselY[0, 2.54 I Z] -
         6.96594 10^7 BesselY[0, 0.11938 I z]
          Log[2.54 Z])) /
     (3.14159 BesselJ[0, 2.54 I Z]
        BesselY[0, 0.11938 I z]^2 -
       3.14159 BesselJ[0, 0.11938 I z]
        BesselY[0, 0.11938 I z]
        BesselY[0, 2.54 I Z])))))
```

$I(x_c) =$

```
(0.9 BesselJ[0, I x]
  BesselY[0, 0.11938 I z]) /
(-1. BesselJ[0, 2.54 I Z]
   BesselY[0, 0.11938 I z] +
   BesselJ[0, 0.11938 I z] BesselY[0, 2.54 I Z]) \
+ (0.9 BesselJ[0, 0.11938 I z] BesselY[0, I x]
   BesselY[0, 2.54 I Z]) /
(1. BesselJ[0, 2.54 I Z] BesselY[0, 0.11938 I z]
    BesselY[0, 2.54 I Z] -
                                                  2
   BesselJ[0, 0.11938 I z] BesselY[0, 2.54 I Z] ))
```

$Z_T = V(x)/I(x) =$


```
(1. BesselJ[0, 0.11938 I z] BesselY[0, I x]
   BesselY[0, 2.54 I Z]
   (-1. BesselJ[0, 2.54 I Z]
      BesselY[0, 0.11938 I z] +
     BesselJ[0, 0.11938 I z] BesselY[0, 2.54 I Z])
   (1. BesselJ[0, 2.54 I Z] BesselY[0, 0.11938 I z]
      BesselY[0, 2.54 I Z] -
     BesselJ[0, 0.11938 I z] BesselY[0, 2.54 I Z]^2 )
   (3.14159 BesselJ[0, 2.54 I Z]
      BesselY[0, 0.11938 I z] -
     3.14159 BesselJ[0, 0.11938 I z]
    BesselY[0, 2.54 I Z] +
   (0.11938 z BesselJ[0, 0.11938 I z]
      BesselY[0, I x]
      (0.375043 z BesselY[0, 2.54 I Z] -
        6.96594 10^7 BesselY[0, 0.11938 I z]
        Log[2.54 Z])) /
     (BesselY[0, 0.11938 I z]
      (3.14159 BesselJ[0, 2.54 I Z]
         BesselY[0, 0.11938 I z]^2 -
        3.14159 BesselJ[0, 0.11938 I z]
         BesselY[0, 0.11938 I z]
         BesselY[0, 2.54 I Z]))))[-1.
   BesselJ[0, I x] (0.375043 z
      BesselY[0, 2.54 I Z] -
     6.96594 10^7 BesselY[0, 0.11938 I z] Log[2.54 Z]
     )]) / (BesselJ[0, I x] BesselY[0, 0.11938 I z])
```